Physics – Uspekhi **66** (8) 775 – 793 (2023)

REVIEWS OF TOPICAL PROBLEMS PACS number: **71.10. – w**

Mean-field concept and post-DMFT methods in the modern theory of correlated systems

Ya S Lyakhova, G V Astretsov, A N Rubtsov

DOI: https://doi.org/10.3367/UFNe.2022.09.039231

Contents

Abstract. We briefly review methods for modeling correlated systems. The concept of correlations is of fundamental physical importance for systems such as Mott–Hubbard insulators, high-temperature superconductors, molecular magnets, and twisted bilayer graphene. With the Hubbard model chosen as a reference, we systematically describe various numerical methods, starting with the mean-field and related theories that map the physical system under study onto an effective interaction-free ensemble. We also discuss the dynamical mean-field theory (DMFT), which is one of the most common modern methods to describe local correlations exactly. DMFT-based diagram methods incorporate effects of nonlocal physics to varying degrees, with the local correlations taken into account in full. In addition, we describe the nondiagram fluctuating local field method, whereby fluctuations of the leading collective modes of the system can be treated nonperturbatively.

Keywords: strongly correlated systems, dynamical mean-field theory, fluctuations

Ya S Lyakhova [1,2,a], **G V Astretsov** [1,3,b], **A N Rubtsov** [1,3,c]
[1] Russian Quantum Center,
Bol'shoi bul'var 30, 121205 Skolkovo, Moscow, Russian Federation
[2] National Research Nuclear University MEPhI
(Moscow Engineering Physics Institute),
Kashirskoe shosse 31, 115409 Moscow, Russian Federation
[3] Lomonosov Moscow State University,
Leninskie gory 1, 119991 Moscow, Russian Federation
E-mail: [a] yanalyakhova@gmail.com, [b] gastretsov@gmail.com,
[c] ar@rqc.ru

Received 14 March 2022, revised 6 September 2022
Uspekhi Fizicheskikh Nauk **193** (8) 825 – 844 (2023)
Translated by S Alekseev

1. Introduction

The many-particle problem in quantum mechanics reduces to solving the Schrödinger equation and in the stationary case can be represented as

$$\left(-\sum_i \frac{\hbar^2\nabla_i^2}{2m} + \sum_{i<j} V(x_i, x_j) + \sum_i v(x_i)\right)\Psi(x_1, x_2, \ldots, x_N) = E\Psi(x_1, x_2, \ldots, x_N), \quad (1)$$

where $V(x_i, x_j)$ is the potential energy of the interaction between the ith and jth particles, $v(x_i)$ is the potential energy of the ith particle in an external field, and $x_i = (\mathbf{r}_i, \sigma_i)$ denotes the spatial position and spin direction of the ith particle.

We consider systems of identical fermions, and hence the wave function $\Psi(x_1, x_2, \ldots, x_N)$ is assumed to be antisymmetric under permutations of its arguments. The term describing the interaction between particles is the source of many interesting physical phenomena and simultaneously the main difficulty in solving the problem. The correlations of electron motion and the collective modes arising as a result of the interaction between particles are important in many-particle systems.

One of the best known examples from the history of correlated materials is the physics of Mott insulators. By the time of Mott's celebrated paper [1], the Bloch–Wilson band theory of conductivity [2], which actually is a mean-field approximation, had already been well developed. According to the Bloch–Wilson theory, current carriers in metals are regarded as a gas of free noninteracting particles moving in the effective field of the lattice and other electrons. The band theory of conductivity predicts metallic behavior for all substances with an odd number of electrons per unit cell of the crystal. In [1], Mott made a number of important remarks, including that some substances, such as nickel oxides, behave

like insulators under certain conditions, although they must be metals according to the band theory of conductivity. In addition, it was noted that these materials have magnetic properties, and, when heated, their insulating behavior is superseded by a metallic one. Later, substances with the above properties became known as *Mott insulators*, and the transition of such substances between metal and insulator phases was called the *Mott transition*. In [1], Mott suggested that this phenomenon could be explained by the Coulomb repulsion of electrons.

Later, in 1963, Hubbard, in a series of studies now known as Hubbard I, Hubbard II, and Hubbard III [3–6], proposed a model that became known as the *Hubbard model*. The goal set by the author, the description of transition 3d-metals, was achieved, notably, at the cost of a number of simplifications. In the original Hubbard model, each lattice site has one s-like orbital, transitions are possible only between nearest neighbors, and the transition amplitudes for all pairs of nearest neighbors are equal. The Hubbard model Hamiltonian has the form

$$\hat{H}_{\mathrm{H}} = -t \sum_{\langle ij\rangle,\sigma} \hat{c}^{\dagger}_{i\sigma}\hat{c}_{j\sigma} - \mu \sum_{j} (\hat{n}_{j\uparrow} + \hat{n}_{j\downarrow}) + U \sum_{j} \hat{n}_{j\uparrow}\hat{n}_{j\downarrow}\,, \quad (2)$$

where $\hat{c}_{i\sigma}$ and $\hat{c}^{\dagger}_{i\sigma}$ are fermion annihilation and creation operators with the spin projection σ at site i, $\hat{n}_{i\sigma} = \hat{c}^{\dagger}_{i\sigma}c_{i\sigma}$ is the particle number operator, and $-t$ corresponds to the electron transition amplitude between adjacent sites $\langle ij\rangle$ and is a matrix element of the Hamilton operator in the basis made of Wannier orbital wave functions. The coupling of two fermions at a site is characterized by U. The number of electrons in the system is determined by the chemical potential (Fermi level) μ; at $\mu = U/2$, half of the maximum possible number of electrons are present in the system. The Hubbard model defined on a square lattice of dimension d has the dispersion law $\varepsilon_{\mathbf{k}} = -2t\sum_{\alpha=1}^{d}\cos k_{\alpha}$ with band width $D = 4dt$. In some cases (in particular, when modeling cuprate compounds), the model also includes hops along the unit cell diagonal; the corresponding coupling is usually denoted by t'. In this review, we restrict ourselves to the case of equilibrium systems characterized by a temperature T (which is measured in energy units here and hereafter; in writing the formulas, we use the system where $e = m = \hbar = 1$).

The Hubbard model has been successfully used to describe Mott insulators. In two extreme cases, the free electron limit ($U \to 0$) and the atomic limit ($t \to 0$), this model can be solved exactly. In the first case, at half filling $n = n_{\uparrow} + n_{\downarrow} = 1$, the model predicts the metal phase, and in the second, the insulator phase. For a long time, the question of the transition from one phase to the other remained unresolved. The complexity of describing the intermediate state is explained by the need to take both local and band physics into account. This regime is called *correlated*. The Hubbard lattice is a starting point for discussing many problems that arise in describing correlation effects. Its generalizations can involve an increase in the number of orbitals at lattice sites, the possibility of hops between distant neighbors [7, 8], and the Coulomb interaction of electrons at different sites [9].

Thus, the Hubbard model is a prototype system in the physics of strong correlations, mainly due to the simplicity of its Hamiltonian. At the same time, Hubbard-class models (typically, multiorbital ones) are also important for computing real compounds, with the parameters of their Hamiltonians determined, for example, based on the results of the density functional method (see Section 2.3). Current interest in strongly correlated systems is, incidentally, due to the discovery in 1986 of high-temperature superconducting (HTSC) cuprates [10], whose description does not fit into the Bardeen–Cooper–Schrieffer framework [11]. It is generally assumed that the appearance of superconductivity in HTSC cuprates is underlain by phenomena associated with electron correlations [12], although there are features in the electron [13] and phonon [14] spectra associated with a significant electron–phonon interaction. In subsequent decades, materials with 'nonconventional' superconductivity based on strontium ruthenate [15] and iron [16] were discovered, and superconductivity in the neighborhood of a quantum critical point was discovered in materials with heavy fermions [17, 18]. The search for possible explanations for superconductivity in these materials also had a significant impact on the development of ideas about quantum spin liquids [19], which are still being actively sought today [20, 21]. More details about materials with strong electron correlations can be found in review [22].

The most recent examples of correlated systems of fermions are atoms in optical traps [23, 24] and flat-band van der Waals heterostructures [25]. A demonstrative example of the latter is provided by twisted bilayer graphene (TBG) [26], which, depending on the angle of relative rotation of the layers and the occupation number, exhibits numerous phases, for example, superconducting regions, Mott insulator and semimetal states, states of integer and fractional topological insulators [27–29], and heavy-fermion phases [30].

The rapid progress and large number of studies in the field of strong correlations has resulted in a situation where many representatives of the broader physics community have some difficulty defining the main methodological results of recent years and assessing the significance of the progress compared to, say, the situation at the end of the 20th century. The available methodological reviews, in our opinion, are aimed at an excessively narrow target audience: the material presented abounds with technical details and, while being without a doubt useful for experts in the field and graduate students working under their supervision, does not provide an 'external' perspective. We believe that publications are needed that play the same role as plenary talks at scientific conferences, i.e., addressed primarily to physicists working in related fields. This review pursues just that goal: we wish to reflect the progress in the mean-field and related approaches in the theory of correlated systems over the entire period of the development of this field. At the same time, the balance of clarity and details of the presentation is in most cases biased toward clarity; for more details, the reader should refer to the references.

We briefly review the mean-field approaches used in modeling systems that can be described in terms of the Hubbard model and its generalizations. Importantly, in our view, the proposed methods by no means exhaust the possible research directions. A significant role in solving problems of the physics of correlated systems is also played by numerically exact schemes. For example, the now 'classic' *exact diagonalization* (ED) method, based on the diagonalization of the Hamiltonian or a numerically accurate search for wave functions and energies of states close to the ground state, is still being actively developed [31–34]. To wit, recently, in [35], the ED scheme was used to study the properties of molecular crystals. A number of papers have been devoted to the study

of TBG using ED [36–39]. The known limitations of the method include, first and foremost, the small lattice size available for calculation due to the computation cost, which grows rapidly as the size increases.

The abundant family of *quantum Monte Carlo* (QMC) *methods* [40–43] must also be mentioned. QMC methods have a reputation as a powerful tool for studying correlated systems [44–46]. The lattice sizes available for calculations with them are somewhat larger than in the case of ED, but researchers face another limitation: the so-called *sign problem*, whose solution remains an urgent task for experts in this field [47–49]. A gratifying approach in this situation is to use the QMC method combined with other schemes. In [50], for example, the low-temperature range in the Hubbard model, inaccessible to QMC due to the sign problem, is studied using the *density matrix renormalization group* (DMRG) method. This combination of methods allowed the authors to reproduce the 'striped' magnetic structure of the system, which is consistent with the experimental data for HTSC cuprates [51]. A wide field for the use of the DMRG in its original form is provided by quasi-one-dimensional systems [52, 53]. In general, the DMRG occupies an important place in the toolbox of numerically exact methods in the physics of correlated systems [54–56] and is often successfully applied to solving problems associated with superconductivity [57–59] and complex strongly correlated systems [60, 61]. We note, however, that the application of the DMRG to 2D and 3D systems remains challenging; currently, active work is underway to improve the method in this regard [62, 63]. It is worth noting the use of tensor networks to describe correlated systems, a direction that has been actively developing in recent years. In particular, renormalization group approaches to the construction of tensor networks allow calculations in the two-dimensional Hubbard model on lattices with sizes up to 10×10, and not only at zero but also at finite low temperatures [64]. Of interest is the possibility of using quantum processors to simulate correlated materials. Modern quantum processors are capable of simulating the magnetic properties of small molecules and clusters based on spin Hamiltonians [65, 66]. However, full simulation of more complex systems requires processors with a large number of long-lived qubits and a high accuracy of single- and multiqubit transformations. The practical feasibility of such projects has become an option due to the introduction of the Bravyi–Kitaev transformation [67] into the computational procedures, which allowed mapping the local fermion operators of a system of m fermionic modes onto $O(\log m)$-qubit transformations in a system of m qubits [68, 69], which in the future can lead to achieving a high computational efficiency of quantum simulators of large-scale correlated systems.

After a brief digression into the methods that remain beyond the scope of this review, we return to our main subject. The review is constructed as follows. We start with a discussion of the family of mean-field methods and the variational principle in Section 2. Mean-field theory and the methods based on it take little or no account of correlation effects. In Section 3, we discuss one of the most popular and powerful numerical approaches to many-particle physics that allows taking local correlations into account: the dynamical mean-field theory (DMFT). Section 4 is devoted to methods that go beyond the DMFT and, to one degree or another, take nonlocal correlation effects of various scales into account. A brief summary is given in Section 5.

2. Mean-field theories

One of the basic approaches to describing many-particle systems is the *mean-field* (MF) *theory*. In the framework of MF methods, the entire interacting problem is reduced to the analysis of some selected collection of degrees of freedom in an effective environment. In the simplest case of stationary MF theory, a many-particle system is reduced to a single mode in an external field. A more complex density functional method in principle allows taking all modes into account, making the description of the system exact, even if limited in practice by the lack of information about the exact form of the density functional. At the same time, the DMFT provides a complete description of a selected site, which ensures that all local effects are taken into account, as we discuss in Section 3.

We start in Section 2.1 with a description of the variational method as a general scheme that allows us to systematically introduce the MF concept.

2.1 Variational method in many-particle problems

When considering problems in quantum mechanics, directly solving the Schrödinger equation often turns out to be impossible. One of the approaches to solving the problem in such cases is the *variational method*. In the simplest formulation, the variational method amounts to considering the ground state energy as a functional of the wave function,

$$E\big[\psi(\zeta)\big] = \big\langle \psi(\zeta)|\hat{H}|\psi(\zeta)\big\rangle\,, \tag{3}$$

where ζ is a parameter of the trial wave function $\psi(\zeta)$. Minimizing (3) yields an approximation for the wave function ψ_0 and the ground state energy E_0.

One of the most celebrated variational methods in the physics of correlated systems is the *Gutzwiller approximation* [70]. The trial Gutzwiller wave function of the Hubbard-model ground state, represented as

$$|\Psi_{\mathrm{G}}\rangle = \prod_{i=1}^{N}(1-\zeta\hat{n}_{i\uparrow}\hat{n}_{i\downarrow})\,|\Psi_0\rangle\,, \tag{4}$$

is constructed so as to describe the decrease in the contribution of states with double filling of sites compared to the contribution of the ground state $|\Psi_0\rangle$ of the noninteracting system. In this scheme, ζ, called the *Gutzwiller parameter*, is found by minimizing the ground state energy. This scheme is interesting in that it allows approaching the description of the Mott transition: a change in the coupling U leads to a change in the sought value of ζ, which makes it possible to smoothly pass from the limit of noninteracting fermions to the atomic limit. As one of the main disadvantages of the Gutzwiller method, we note the difficulty in controlling the error and the possibility of improving the result obtained.

In many cases, instead of a trial wave function, it may be easier to introduce a trial Hamiltonian whose eigenfunctions and spectrum can be calculated explicitly. It is then often convenient to use the *Gibbs–Bogoliubov–Feynman* (GBF) *inequality* [71], which minimizes the free energy $F = -T\ln\mathrm{Tr}\exp(-\hat{H}/T)$ and is therefore applicable to systems at a finite temperature. The GBF inequality has the form

$$F \leqslant F' + \langle \hat{H} - \hat{H}'\rangle'\,, \tag{5}$$

where primed quantities refer to the trial ensemble for which the solution is known, and $\langle\ldots\rangle'$ denotes thermodynamic

averaging over this ensemble. A detailed derivation of (5) can be found in book [72]. Inequality (5) allows obtaining an upper bound for the free energy and minimizing it by varying the parameters of the trial Hamiltonian $\hat{H}'(\zeta)$. The equation for the optimal value of the variational parameter ζ_0 then becomes

$$\delta F\big|_{\zeta_0} = 0\,. \tag{6}$$

2.2 Mean-field theory

We formulate the stationary MF theory in the context of the variational method. The effective field can then be regarded as a free parameter of the trial MF Hamiltonian and its value can be chosen by varying free energy (5).

We show how this procedure is applied to the Hubbard model, with each site feeling the action of the external magnetic field h_j directed along the z-axis. The Hamiltonian of the system has the form $\hat{H} = \hat{H}_{\rm H} - \sum_j h_j(\hat{n}_{j\uparrow} - \hat{n}_{j\downarrow})$, where $\hat{H}_{\rm H}$ is the Hubbard model Hamiltonian, Eqn (2). We write the trial Hamiltonian in the form

$$\hat{H}_{\rm MF} = -t\sum_{\langle ij\rangle,\,\sigma}\hat{c}^{\dagger}_{i\sigma}\hat{c}_{j\sigma} - \sum_j h_j^{\rm eff}(\hat{n}_{j\uparrow} - \hat{n}_{j\downarrow})\,, \tag{7}$$

where $h_j^{\rm eff}$ is the effective magnetic field. The GBF inequality (5) then takes the form

$$\begin{aligned} F \leqslant\ & -T\ln Z_{\rm MF} + \sum_j \big\langle U\hat{n}_{j\uparrow}\hat{n}_{j\downarrow} - \mu(\hat{n}_{j\uparrow} + \hat{n}_{j\downarrow}) \\ & + (h_j^{\rm eff} - h_j)(\hat{n}_{j\uparrow} - \hat{n}_{j\downarrow})\big\rangle_{\rm MF}\,, \end{aligned} \tag{8}$$

where $Z_{\rm MF} = {\rm Tr}\exp(-\hat{H}_{\rm MF}/T)$.

We note that $-T\,\delta\ln Z_{\rm MF} = -\langle\hat{n}_{j\uparrow} - \hat{n}_{j\downarrow}\rangle_{\rm MF}\,\delta h_j^{\rm eff}$, and, because the trial ensemble is noninteracting, i.e., Gaussian, it follows that $\langle\hat{n}_{j\uparrow}\hat{n}_{j\downarrow}\rangle_{\rm MF} = \langle\hat{n}_{j\uparrow}\rangle_{\rm MF}\langle\hat{n}_{j\downarrow}\rangle_{\rm MF}$. Next, varying the magnetic field does not change the on-site charge states: $\delta\langle\hat{n}_{j\uparrow}\rangle_{\rm MF} = -\delta\langle\hat{n}_{j\downarrow}\rangle_{\rm MF}$. Taking these relations into account, we apply condition (6) to (8) to obtain the well-known result

$$h_j^{\rm eff} = h_j + \frac{U}{2}\langle\hat{n}_{j\uparrow} - \hat{n}_{j\downarrow}\rangle_{\rm MF}\,. \tag{9}$$

Equation (9) can be solved, for example, by iterations, at each step calculating

$$\langle\hat{n}_{j\sigma}\rangle_{\rm MF} = Z_{\rm MF}^{-1}\,{\rm Tr}\left[\hat{n}_{j\sigma}\exp\left(-\frac{\hat{H}_{\rm MF}}{T}\right)\right]$$

and updating $h_j^{\rm eff}$.

We consider the case of a uniform external magnetic field $h_j = h$. Then, the trial system is a collection of two ensembles of electrons, with opposite z-components of spins, characterized by the effective chemical potentials $\mu - h^{\rm eff}$ and $\mu + h^{\rm eff}$. Because a change in the chemical potential leads to a change in the concentration that at low temperatures is proportional to the density of states $\rho(\mu)$ near the Fermi level, it follows that $\langle\hat{n}_{\uparrow} - \hat{n}_{\downarrow}\rangle_{\rm MF} = 2h^{\rm eff}\rho(\mu)$. Thus, the susceptibility in the ferromagnetic channel in the MF approximation is given by

$$\chi^{\rm F} \equiv \frac{\partial\langle\hat{n}_{\uparrow} - \hat{n}_{\downarrow}\rangle_{\rm MF}}{\partial h} = \frac{2\rho(\mu)}{1 - \rho(\mu)U}\,. \tag{10}$$

For $\rho(\mu)U = 1$, the susceptibility diverges, which corresponds to the spontaneous appearance of ferromagnetic ordering. Expression (10) is called the *Stoner criterion*. In 1938, Stoner formulated a condition that determines whether a material with a given band structure is ferromagnetic [73]. As follows from the Stoner condition, materials with a high density of states at the Fermi level are ferromagnetic, which explains why transition metals with an unfilled d-shell, such as Fe, Ni, and Co, are ferromagnetic.

2.3 Density functional method

An important example of the development of the idea of reducing a many-particle problem to a single-particle one is the *density functional theory* (DFT), currently one of the most popular methods in quantum materials science and quantum chemistry [74, 75]; it is theoretically exact and shows good agreement with experimental data [76, 77].

The DFT is based on the Hohenberg–Kohn theorem [78], which states that, given the particle number density in the ground state, $n(\mathbf{r})$, one can uniquely determine the ground-state wave function ψ_0. Technically, this allows representing any quantities characterizing the system as density functionals of the number of particles. Further, Kohn and Sham showed that the spatial density distribution of system (1) with the Coulomb interaction $V(\mathbf{r}_1, \mathbf{r}_2) = 1/|\mathbf{r}_1 - \mathbf{r}_2|$ can be reproduced exactly if we consider a system of noninteracting particles in the potential

$$\hat{V}_{\rm s} = v(\mathbf{r}) + \int\frac{n(\mathbf{r}')}{|\mathbf{r} - \mathbf{r}'|}\,{\rm d}^3\mathbf{r}' + \hat{v}_{\rm xc}\,, \tag{11}$$

where the first term on the right-hand side, $v(\mathbf{r})$, is the external potential acting on the system, the second term is the averaged potential of the electrons that make up the system, and the *exchange–correlation energy* $\hat{v}_{\rm xc}$ formally includes all multiparticle effects. In accordance with the Hohenberg–Kohn theorem, $\hat{v}_{\rm xc}$ is uniquely determined by the system density $n(\mathbf{r})$.

We emphasize that, from the mathematical standpoint, $\hat{v}_{\rm xc}$ is an unknown density functional of the system. The success of the DFT is due to the existence of good approximations for this functional dependence. For example, in the *local density approximation* (LDA), $\hat{v}_{\rm xc} = v_{\rm xc}(\mathbf{r})$ is determined only by the density at a given point $\mathbf{r}$ (and not at all points of the system, as should be the case in the exact theory).

Practical calculations using the DFT consist in iteratively solving the Kohn–Sham equations — the Schrödinger equation for noninteracting particles in the effective field that depends on their density. At some step of the procedure, given the effective potential $\hat{V}_{\rm s}$, one finds the density of the system of noninteracting fermions located in the field of that potential. This problem reduces to solving the one-particle Schrödinger equation $\hat{H}_{\rm KS}\psi_i(\mathbf{r}) = \varepsilon_i\psi_i(\mathbf{r})$ with the Hamiltonian

$$\hat{H}_{\rm KS} = -\frac{\hbar^2}{2m}\nabla^2 + \hat{V}_{\rm s}\,.$$

Then, based on the found density $n(\mathbf{r}) = \sum_i|\psi_i(\mathbf{r})|^2$, where the sum is taken over the occupied states, one constructs a new effective potential, and so on until the iterations converge.

The DFT method developed for *ab initio* Hamiltonians can be used to construct model lattice systems, in particular, to find the t and U parameters of the Hubbard model [79, 80].

However, directly applying the DFT to the description of the Hubbard lattice itself requires a corresponding reformulation of the Hohenberg–Kohn theorem and the Kohn–Sham equations, as was done in [81].

By constructing the original theory, the DFT method is designed to determine the properties of the ground or equilibrium state. The eigenvalues ε_i of the Hamiltonian $\hat{H}_{\mathrm{KS}}$, initially introduced as auxiliary quantities, are often used in practice to compute the band structure of materials, sometimes with good results (see Fig. 2 in Section 2.4). In what follows, we are interested in single-particle excitations of thermodynamically equilibrium systems. To analyze them, we use the Green's function in the Matsubara representation [82, 83],

$$G_{\nu\mathbf{r}\mathbf{r}'} = -\int_0^{1/T} \left\langle \hat{c}_{\mathbf{r}}(\tau)\hat{c}^{\dagger}_{\mathbf{r}'}(0)\right\rangle \exp(\mathrm{i}\nu\tau)\,\mathrm{d}\tau\,,$$

where $\nu = (2j+1)\pi T$, j is an integer, and $\hat{c}(\tau) = \exp(\tau\hat{H}) \times \hat{c}\exp(-\tau\hat{H})$. The noninteracting ensemble is characterized by the Green's function

$$G_{0,\,\nu\mathbf{r}\mathbf{r}'} = \sum_j \frac{\psi_j^*(\mathbf{r}')\psi_j(\mathbf{r})}{\mathrm{i}\nu - \varepsilon_j}\,, \tag{12}$$

where ψ_j and ε_j are single-particle wave functions and energies obtained within the DFT by solving the Kohn–Sham equations.

If the system under consideration has translation invariance, and if it is specifically defined on a simple lattice, then its Green's function depends only on the difference between the spatial arguments $\mathbf{r} - \mathbf{r}'$, and it is natural to move to the Fourier transform of the Green's function $G_{\nu\mathbf{k}}$. The Kohn–Sham equations are then solved by plane waves with the dispersion law $\varepsilon_{\mathbf{k}}$, and the Green's function in the DFT approximation has the form

$$G_{0,\,\nu\mathbf{k}} = \frac{1}{\mathrm{i}\nu - \varepsilon_{\mathbf{k}}}\,. \tag{13}$$

The use of the Matsubara representation requires further comments. We use it here and below for the uniformity of presentation, because, for the DMFT family methods (see Sections 3 and 4), computations of equilibrium systems are actually done only in this representation. However, the real spectrum of electron excitations is determined by the density of states $A(\omega) = -(1/\pi)\sum_{\mathbf{k}} \mathrm{Im}\, G_{\omega\mathbf{k}}$, where $G_{\omega\mathbf{k}}$ is the Green's function at real frequencies. (Here and hereafter, the symbol for the summation over momenta includes the factor $1/N$, where N is the number of lattice sites, and hence $\sum_{\mathbf{k}} 1 = 1$. Similarly, summation over Matsubara frequencies includes the factor T.) The function $G_{\omega\mathbf{k}}$ can be obtained by an analytic continuation of $G_{\nu\mathbf{k}}$; in the above formulas, this continuation corresponds to the substitution $\mathrm{i}\nu \to \omega + \mathrm{i}0$.

2.4 *GW* method

The DFT calculations of the electron spectrum are insufficient in many cases: interaction effects lead to a renormalization of the excitation spectrum, which formally corresponds to the appearance of the self-energy $\Sigma_{\nu\mathbf{k}}$ defined by the relation $G^{-1}_{\nu\mathbf{k}} = G^{-1}_{0,\,\nu\mathbf{k}} - \Sigma_{\nu\mathbf{k}}$. A significant part of the studies of correlated systems is devoted specifically to the calculation of the renormalization of their electron spectrum.

A possible avenue for further development is offered by perturbative methods, starting from the DFT result as the zeroth approximation. As an example of this approach, we consider the *GW method*. This is a perturbative diagram method (Fig. 1) in which the self-energy function Σ is expanded into a perturbative series in the screened Coulomb interaction W, and only the first term of the expansion is preserved (for simplicity, we write equations for a translation invariant system),

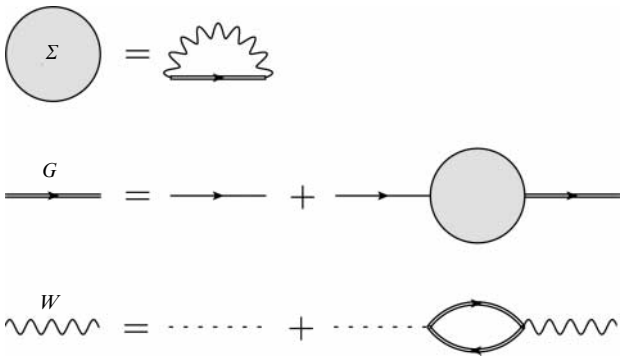

Figure 1. Block diagrams of the GW method: self-energy Σ in the GW approximation, the Dyson equation relating Green's function G and the self-energy, and the equation for screened interaction W in the random-phase approximation.

$$\Sigma_{\nu\mathbf{k}} = -\sum_{\Omega\mathbf{q}} G_{\nu-\Omega,\,\mathbf{k}-\mathbf{q}} W_{\Omega\mathbf{q}}\,, \tag{14}$$

where $W_{\Omega\mathbf{q}}$ is the Fourier transform of W. We note that, in contrast to the Fourier transform of the Coulomb interaction $\mathrm{V}_{\mathbf{q}}$, $W_{\Omega\mathbf{q}}$ also depends on the bosonic Matsubara frequencies Ω, thus defining not only the screening but also the retardation.

For the screened interaction, we can use the random phase approximation [84]:

$$W_{\Omega\mathbf{q}} = V_{\mathbf{q}} + \sum_{\nu\mathbf{k}} V_{\mathbf{q}} G_{\Omega-\nu,\,\mathbf{q}-\mathbf{k}} G_{\nu,\,\mathbf{k}} W_{\Omega\mathbf{q}}\,. \tag{15}$$

The above expressions for Σ, G, and W make up a self-consistent system of equations. If the starting point is G_0, taken from calculations by the DFT method, then, in order to avoid double counting of the interaction effects, we must subtract the exchange–correlation potential from the GW self-energy, and hence the Green's function becomes

$$G_{\nu\mathbf{k}} = \frac{1}{G^{-1}_{0,\,\nu\mathbf{k}} + v_{\mathrm{xc}} - \Sigma_{\nu\mathbf{k}}}\,, \tag{16}$$

where v_{xc} is the exchange–correlation energy (a constant in the spatially homogeneous case).

Figure 2 shows a comparison of the results of DFT and GW calculations of the band gap for various substances. The LDA gives the band gap of the correct order of magnitude for many materials, but systematically underestimates its value quantitatively. It can be seen from the figure that the GW approximation significantly increases the LDA accuracy. However, the method predicts nonphysical effects near the atomic limit and also suffers from the self-screening problem [85, 86]. To overcome these difficulties, the GW method can be combined, for example, with corrections to vertex functions, which corresponds to taking quantum effects into account in the exchange–correlation component of the self-energy function Σ [87, 88].

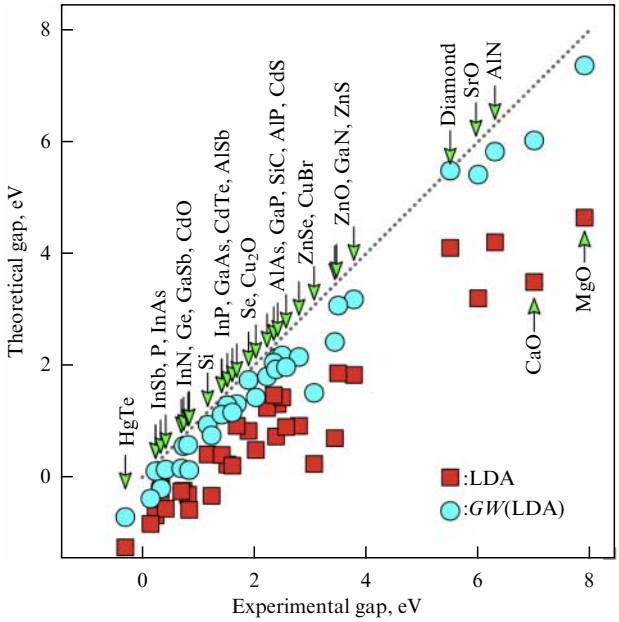

Figure 2. Comparison of theoretical and experimental values of the band gap for semimetals (left-hand side, negative gap), semiconductors (middle part), and insulators (right-hand side) obtained in the DFT (red squares) and *GW* (blue dots) frameworks [89].

3. Accounting for local correlations

The *GW* method, which is limited to only one self-energy diagram, is not applicable to strongly correlated systems, for example, to the description of Mott transitions. The minimal description of Mott physics seems to require explicitly including the many-particle effects associated with the presence of Hubbard terms in the Hamiltonian, as is done, for example, in the Gutzwiller approach. We also note the LDA + U method [90], where a simple functional correction to the LDA result allows taking correlations into account at the static level. The LDA + U method actually turns out to be useful in practical calculations of the properties of transition and rare-earth metal compounds with moderate correlations.

A major breakthrough in this area was paper [91], where, based on the MF approximation, a generalized version of the LDA + U method was developed in the limit of a large coordination number, called the *local-impurity self-consistent approximation* (LISA). Later, the method became known as the DMFT, emphasizing the possibility of accurately taking local correlations into account in that framework.

We first consider a method that is ideologically related to the DMFT and which had appeared somewhat earlier, the coherent potential approximation in the theory of inhomogeneous systems.

3.1 Anderson model. Coherent potential approximation

The *Anderson model* in general describes a class of systems with so-called diagonal disorder. The Hamiltonian of such a system can be expressed as

$$\hat{H} = -t \sum_{\langle ij \rangle} \hat{c}_i^{\dagger} \hat{c}_j + \sum_i v_i \hat{n}_i \,, \tag{17}$$

where v_i is a random potential at the ith site with specific values corresponding to some probability distribution. For example, for a model of a binary substitutional alloy whose lattice is made of two types of sites, A and B, the potential takes one of the two random values v^{A} and v^{B}. The v_i on different sites are not correlated. We pose the problem of finding the Green's function of such a system, averaged over realizations of the random potential.

A convenient approach to solving the Anderson model is the *coherent potential approximation* (CPA) [92]. The idea of the CPA is to consider an auxiliary system given by a collection of isolated *impurity problems* — decoupled sites, each of which feels a random potential v_i and the effective hybridization Δ. The latter is determined so as to best describe the average effect exerted on a given site by its neighbors on the original lattice (17). Physically, it is important that this effect be delayed: the lattice response is determined by the state of the site not only at the current time but also at earlier times. This corresponds to a frequency-dependent hybridization $\Delta = \Delta_\nu$. The impurity problem thus becomes non-Hamiltonian and is described by the action written in terms of Grassmann variables $c_\nu^{\dagger}$ and c_ν [84, 93]:

$$\mathcal{S}[c_j^{\dagger}, c_j] = \sum_\nu c_\nu^{\dagger}(-\mathrm{i}\nu + v_j + \Delta_\nu) c_\nu \,. \tag{18}$$

We write the impurity Green's function averaged over the realizations of v as

$$\mathcal{G}_\nu = \left\langle \frac{1}{\mathrm{i}\nu - v_j - \Delta_\nu} \right\rangle_v \equiv \sum_v \frac{p(v)}{\mathrm{i}\nu - v - \Delta_\nu} \,, \tag{19}$$

where $p(v)$ defines the probability distribution for random impurities. The practical calculation of $\mathcal{G}_\nu$ is straightforward: for example, for a binary alloy, the sum in (19) contains only two terms. The impurity self-energy

$$\Sigma_\nu = \mathrm{i}\nu - \Delta_\nu - (\mathcal{G}_\nu)^{-1} \tag{20}$$

determines how disorder modifies the Green's function of the impurity problem 'on average.' The basic assumption of the CPA method is that, for the original problem (17), on average, disorder leads to the same effect: the lattice Green's function can be expressed as

$$G_{\nu\mathbf{k}} = \frac{1}{\mathrm{i}\nu - \varepsilon_{\mathbf{k}} - \Sigma_\nu} \,. \tag{21}$$

The above system of equations is additionally subjected to the condition that the properties of the lattice sites be modeled by the impurity problem in the best way possible. For this, we require that the Green's functions of the original and auxiliary problems locally coincide: $\mathcal{G}_\nu = \sum_{\mathbf{k}} G_{\nu\mathbf{k}}$. This equality is the self-consistency condition of the method, stating that the Δ_ν hybridization must be chosen such that the condition holds at any Matsubara frequency.

This method successfully predicts the optical and transport properties of alloys [92]. Importantly, the method has an MF nature: in fact, for each site, the disordered environment is replaced by an averaged one, described by the Δ_ν hybridization (Fig. 3). Accordingly, the CPA does not take nonlocal correlations into account, which complicates its use in those cases where the environment of each site strongly fluctuates, as in lower-dimensional systems and in Anderson insulators [94, 95]. In addition, the CPA does not reproduce the corrections to conductivity at low temperatures due to weak localization, and it also entails difficulties for systems with off-diagonal disorder [92].

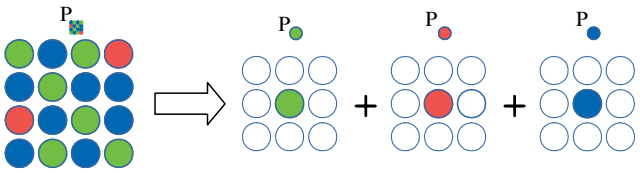

Figure 3. In the CPA framework, a system with disorder is replaced with an ensemble of problems for each type of impurity with weights corresponding to how often a given impurity occurs in the alloy.

3.2 Dynamical mean-field theory

The DMFT is one of the most important methods for describing correlated systems and allows accurately describing local on-site fluctuations. We first consider a system of self-consistent DMFT equations using Hubbard model (2) as an example, with the Hamiltonian conveniently represented as

$$\hat{H}_{\mathrm{H}} = \sum_j \hat{H}_j^{\mathrm{at}} + \sum_{\mathbf{k}\sigma} \varepsilon_{\mathbf{k}} \hat{c}^{\dagger}_{\mathbf{k}\sigma} \hat{c}_{\mathbf{k}\sigma} \,, \tag{22}$$

where $\hat{H}_j^{\mathrm{at}} = U\hat{n}_{j\uparrow}\hat{n}_{j\downarrow} - \mu(\hat{n}_{j\uparrow} + \hat{n}_{j\downarrow})$ is the Hamiltonian of an isolated Hubbard atom.

We first introduce the basic DMFT equations without formal justification, as we did in Section 3.1 for the CPA, and then show how these equations can be obtained from a variational principle. As in the derivation of the CPA equations, we introduce an auxiliary system given by a collection of impurity problems, each of which corresponds to a lattice site with an effective hybridization Δ_ν, the so-called *Anderson impurity model* (AIM). The action of the impurity problem is given by

$$\mathcal{S}[c_j^{\dagger}, c_j] = S^{\mathrm{at}}[c_j^{\dagger}, c_j] + \sum_{\nu} c^{\dagger}_{\nu j\sigma} \Delta_\nu c_{\nu j\sigma} \,, \tag{23}$$

where $S^{\mathrm{at}}[c_j^{\dagger}, c_j]$ is the action of a Hubbard atom corresponding to the Hamiltonian $\hat{H}_j^{\mathrm{at}}$. To simplify the formulas, we assume that the system symmetry is not broken, i.e., the hybridization is the same for all sites and is independent of spin.

We now have to find the Green's function $\mathcal{G}$ of the impurity problem. In the case of the CPA, the Green's function could be found analytically, but for hybridization of a general form, such a problem does not allow an analytic solution. However, there are algorithms and numerous software implementations, so-called AIM *solvers*, that allow solving the impurity problem numerically rather efficiently [96–100]. We note one more difference between the CPA and DMFT. In the CPA, as follows from (19), a change in hybridization at some frequency leads to a change in the impurity problem Green's function only at the same frequency, whereas, in the DMFT, $\mathcal{G}_\nu$ is a functional of the hybridization Δ_ν, defined for the entire frequency spectrum.

If the Green's function of the impurity problem is known, then it is easy to find the self-energy $\Sigma_\nu = \mathrm{i}\nu + \mu - \Delta_\nu - \mathcal{G}_\nu^{-1}$. Substituting Σ_ν for the lattice self-energy, we again obtain an expression for the DMFT lattice Green's function, which coincides with (21). The Green's function can also be expressed as

$$G_{\nu\mathbf{k}} = \frac{1}{\mathcal{G}_\nu^{-1} + \Delta_\nu - \varepsilon_{\mathbf{k}}} \,. \tag{24}$$

Equation (24) must be supplemented with the self-consistency condition

$$\mathcal{G}_\nu = \sum_{\mathbf{k}} G_{\nu\mathbf{k}} \,. \tag{25}$$

In practical implementations of the method, an iterative procedure is followed. The first step consists in adopting some assumption about the hybridization function, for example, setting $\Delta_\nu = 0$. At the nth iteration, hybridization changes according to the rule

$$\Delta_\nu^{(n+1)} = \Delta_\nu^{(n)} + \xi\left(\sum_{\mathbf{k}} G_{\nu\mathbf{k}}^{(n)}\right)^{-1} - \xi\left(\mathcal{G}_\nu^{(n)}\right)^{-1} \,,$$

where the Green's functions of the lattice and impurities are obtained for the hybridization $\Delta^{(n)}$ by the method described above, and $\xi \sim 1$ is a parameter of the numerical procedure that must be chosen so as to ensure the best convergence of iterations. It is easy to see that a fixed point of such a transformation corresponds to the satisfaction of condition (25). It can also be shown that, in the limit of a noninteracting system, the described procedure with $\xi = 1$ already leads to a solution after the first iteration.

We must now reconsider the question of the use of the Matsubara representation. Like the methods described above, the DMFT equations can be formulated using both Matsubara and real frequencies. However, numerical schemes for solving the Anderson impurity problem turn out to be much easier to implement for the Matsubara representation (a discussion of the sources of difficulties associated with the so-called sign problem and modern progress in solving them can be found in [101, 102]); in practice, therefore, DMFT calculations for equilibrium systems are always performed in the Matsubara representation. There are methods that allow analytically continuing numerical results to the real frequency axis [103, 104] (although such a problem is ill defined) and thereby construct the spectrum of the density of states of the system.

From the standpoint of diagram techniques, the DMFT can be considered an approximation in the sense that the diagram series pertain not to the entire lattice but to a single site. Accordingly, when calculating the self-energy, the full set of diagrams is taken into account, but for each of them, instead of summing over all positions of the internal sites, only one of them is taken (Fig. 4). If we recall that the probability of hopping from site to site (nonlocal effect) decreases in inverse proportion to the coordination number Z, it becomes clear that the self-energy function becomes purely local in the large-Z limit. In other words, the DMFT is an exact method in the limit $Z \to \infty$.

We now show how the DMFT equations can be obtained using the GBF variational method. The action corresponding to the Hubbard model Hamiltonian can be represented as

$$S[c^{\dagger}, c] = \sum_j \mathcal{S}[c_j^{\dagger}, c_j] + \sum_{\nu\mathbf{k}\sigma} c^{\dagger}_{\nu\mathbf{k}\sigma}(\varepsilon_{\mathbf{k}} - \Delta_\nu) c_{\nu\mathbf{k}\sigma} \,, \tag{26}$$

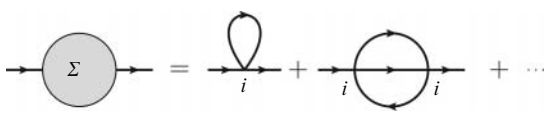

Figure 4. DMFT self-energy is the sum of all local Feynman diagrams.

where we took into account that $\sum_j c^{\dagger}_{vj\sigma} c_{vj\sigma} = \sum_{\mathbf{k}} c^{\dagger}_{v\mathbf{k}\sigma} c_{v\mathbf{k}\sigma}$; the impurity model action $\mathcal{S}[c_j^{\dagger}, c_j]$ is defined by formula (23). We consider the Gaussian approximation for $\mathcal{S}[c_j^{\dagger}, c_j]$, which exactly reproduces the free energy

$$\mathcal{F} = -T \ln \int \exp\left(-\mathcal{S}[c_j^{\dagger}, c_j]\right) \mathcal{D}[c_j^{\dagger}, c_j]$$

and the impurity problem Green's function

$$\tilde{\mathcal{S}}[c_j^{\dagger}, c_j] = \frac{\mathcal{F}}{T} - \sum_{v\sigma} \left(c^{\dagger}_{vj\sigma} \mathcal{G}_v^{-1} c_{vj\sigma} - \ln \mathcal{G}_v \right). \tag{27}$$

The DMFT approximation can be regarded as the result of replacing $\mathcal{S}[c_j^{\dagger}, c_j]$ in lattice action (26) with approximate expression (27)

$$\tilde{S}[c^{\dagger}, c] = \frac{N\mathcal{F}}{T} - \sum_{v\mathbf{k}\sigma} \left[(\mathcal{G}_v^{-1} + \Delta_v - \varepsilon_{\mathbf{k}}) c^{\dagger}_{v\mathbf{k}\sigma} c_{v\mathbf{k}\sigma} - \ln \mathcal{G}_v \right]. \tag{28}$$

As can be seen, approximation (28) indeed corresponds to the Green's function (24). We can hence also obtain the DMFT approximation for the free energy of the system. After substituting $\tilde{S}$, integration gives

$$F = N\mathcal{F} + T \sum_{v\mathbf{k}\sigma} \ln \frac{G_{v\mathbf{k}}}{\mathcal{G}_v}. \tag{29}$$

In tensor notation, the second term on the right-hand side of (29) can be written as $-T \ln[1 + \mathcal{G}(\Delta - \varepsilon)]$.

In accordance with the GBF variational principle, we require that F be invariant under small variations in Δ. We have to calculate the total variation, i.e., take into account that varying the hybridization $\delta\Delta$ entails varying the self-energy $\delta\Sigma$. The calculation leads to the equation

$$\sum_{\mathbf{k}} (G_{v\mathbf{k}} - \mathcal{G}_v)\, \delta\Sigma_v = 0. \tag{30}$$

Because the variation $\delta\Sigma$ can be arbitrary, self-consistency condition (25) follows from Eqn (30).

Being a formally exact method in the limit of a large coordination number, the DMFT has been successfully used to describe many real systems. In particular, this method ensures a good description of the above-mentioned Mott transitions caused by the Coulomb repulsion of electrons at lattice sites [105, 106]. Various hybrid schemes, for example, GW + (E)DMFT [107–109], also provide options for solving physical problems.

Finally, we note that the DMFT method can easily be generalized to the case of symmetry broken either spontaneously or by external fields. The hybridization then remains spatially local, but turns out to depend on the spin and the lattice site number, and may in addition contain anomalous components, which motivates rewriting the formulas in tensor form. In particular, the Green's function then takes the form

$$G = \frac{1}{\mathcal{G}^{-1} + \Delta - \varepsilon}, \tag{31}$$

where the tensors $\mathcal{G}$ and Δ are diagonal in the (r, v) representation but have off-diagonal spin components. On the contrary, the ε tensor is diagonal in spin and frequency indices in this representation, but is not diagonal with respect to the coordinate indices. Self-consistency condition (25) then implies that the diagonal components of the lattice Green's function in the coordinate representation coincide with the solution to the impurity problem at each site.

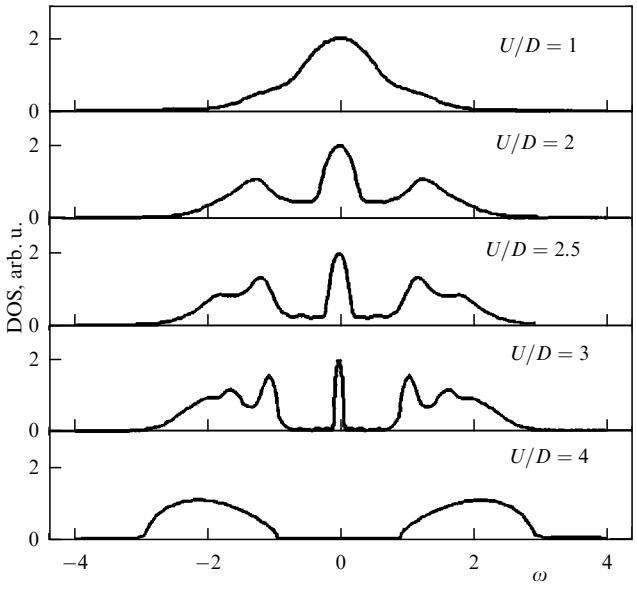

Figure 5. Spectral density (density of states, DOS) as a function of real frequency ω for different ratios U/D of the interaction strength to the band width, calculated using the DMFT. Four top curves correspond to the metal case, bottom curve ($U/D = 4$) corresponds to an insulator. For intermediate values of U, a peak at $\omega = 0$, which is characteristic of a single-site DMFT [111], is clearly visible.

It is worth mentioning one of the DMFT problems, which is typical for one-site impurity problems. It follows from Luttinger's theorem that, if the self-energy of a Fermi liquid is local, then its density of states at the Fermi level is independent of the interaction strength. It follows from such pinning of the density of states at the Fermi level that, for metal systems close to the Mott transition, the DMFT predicts a peak, characteristic of the Kondo problem, at the center of the emerging Mott band gap (Fig. 5); this peak exists as long as the system remains a Fermi liquid. Being an artifact of the method, the peak does not give rise to additional difficulties in predicting the properties of real materials, however [110]. This artifact disappears when using multi-orbital models or cluster methods, which are described in Section 3.3.

Cases of successful use of the DMFT include, in particular, the description of the Mott-insulator–metal phase transition in vanadium oxide V_2O_3 doped with chromium [112]. It is known from experimental data [113] that V_2O_3 is an insulator. Doping V_2O_3 with chromium increases the electron mobility, which leads to a decrease in the effective Coulomb repulsion between electrons. The DFT incorrectly predicts the metallic state for underdoped V_2O_3. Figure 6 shows the densities of states for V_2O_3 calculated using the LDA and LDA + DMFT methods. The density functional method gives a nonzero density of states at the Fermi level and incorrectly predicts undoped vanadium oxide to be a metal. However, the combination of the density functional theory with the DMFT, LDA + DMFT, shows a transition from the metal to the Mott insulator with an increase in the Hubbard interaction U. We also see in Fig. 6 that the characteristic width of the LDA + DMFT spectral function is larger than for the LDA method. This is related

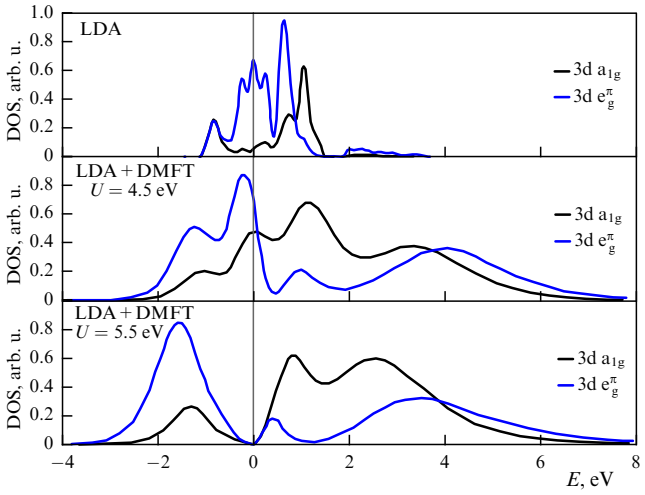

Figure 6. Spectral density as a function of energy E calculated using the LDA and LDA + DMFT methods at two Hubbard interaction strengths $U = 4.5$ and 5.5 eV for the Mott insulator V_2O_3. $E = 0$ corresponds to the Fermi energy, black and blue curves refer to the respective orbital states a_{1g} and e_g^π. LDA erroneously predicts the final density of states at the Fermi level (metal), while LDA + DMFT with a sufficiently large $U = 5.5$ eV predicts a gap in the density of states (insulator) [112].

to the renormalization of the effective mass of the density of states, which follows from the frequency dependence of the self-energy Σ_ω. Among the recent achievements of the DMFT, it is worth noting its application to two-layer twisted structures, in particular, WSe_2 and $MoTe_2/WSe_2$, whose magnetic and metal–insulator phases are successfully described within this approach [114].

3.3 Cluster generalizations of the dynamical mean-field theory

Cluster methods are based on the idea of approximating the entire lattice with a large number of degrees of freedom by a small cluster placed in an effective environment simulating the remaining degrees of freedom [115]. The cluster DMFT scheme is in many respects similar to the one-particle scheme. First, the cluster degrees of freedom are determined and the exact Green's function and self-energy function are found. Then, the self-consistency condition is formulated. At the final stage, the relation between the cluster and lattice self-energy functions is established [116].

The main methodological problem of cluster methods is that the choice of the effective hybridization and hence the relation between the lattice and cluster Green's functions is ambiguous. Various cluster schemes are known. We confine ourselves to a brief comparison of the most common approaches; a detailed analysis of various cluster methods and a comparison with the results of other well-known approaches can be found, for instance, in reviews [115, 117].

The simplest cluster scheme is the so-called *cellular DMFT* (CDMFT). In the CDMFT approach, the original system is represented as a superlattice, each of whose cells contains several lattice sites of the original system. For example, in the simplest version of the Hubbard model, cells of 2×2 atoms are selected, after which one-site DMFT equations can be used, with each superlattice cell regarded as a multiorbital system hybridized by a self-consistent field. By construction, the CDMFT takes intersite correlations into account within each superlattice cell. This inclusion of nonlocal effects, even if partial, allows the CDMFT to yield a number of results that are unavailable in the one-site scheme [118, 119]. In particular, unlike the DMFT, CDMFT shows the formation of a pseudogap preceding the Mott transition [120, 121] (Fig. 7). In one of the possible modifications [122], the CDMFT with 2×2 clusters predicts d-wave superconductivity in the doped Hubbard model.

However, the CDMFT suffers from a number of disadvantages associated with the artificial violation of periodicity when the initial system is divided into clusters. In particular, except for the minimum 2×2 cell, the CDMFT cluster sites turn out to be nonequivalent: one part of them belongs to the cluster boundary and the other part is located inside it. This problem is solved in the *dynamical cluster approximation* (DCA) method [123–125], where periodic boundary conditions are introduced for cluster sites, such that the cluster wave vector ranges the values from the discrete series $\mathbf{K}_{x,y} = 2\pi j_{x,y}/L_{x,y}, 0 \leqslant j_{x,y} < L_{x,y}$, with the overall cluster size $N_c = L_x \times L_y$. The wave vector of the original lattice can be represented as $\mathbf{k} = \mathbf{K} + \tilde{\mathbf{k}}$, where $|\tilde{k}_{x,y}| < \pi/L_{x,y}$. The self-energy in the original lattice problem is assumed to depend only on $\mathbf{K}$, $\Sigma_{\nu,\mathbf{K}+\tilde{\mathbf{k}}} = \Sigma_{\nu\mathbf{K}}$, and coincide with the cluster self-energy. Thus, the Green's function of the complete problem has the form

$$G_{\nu\mathbf{k}} = G_{\nu,\mathbf{K}+\tilde{\mathbf{k}}} = \frac{1}{\mathrm{i}\nu - \varepsilon_{\mathbf{K}+\tilde{\mathbf{k}}} - \Sigma_{\nu\mathbf{K}}}. \tag{32}$$

The DCA is therefore said to lead to a coarse-graining of the space of wave vectors.

Given some hypothesized $\Sigma_{\nu\mathbf{K}}$ and hence $G_{\nu,\mathbf{K}+\tilde{\mathbf{k}}}$, we can construct a coarse-grained Green's function

$$\tilde{G}_{\nu\mathbf{K}} = \frac{N_c}{N}\sum_{\tilde{\mathbf{k}}} G_{\nu,\mathbf{K}+\tilde{\mathbf{k}}}.$$

The impurity problem then has the hybridization $\Delta_{\nu\mathbf{K}} = \mathrm{i}\nu - \varepsilon_{\mathbf{K}} - \Sigma_{\nu\mathbf{K}} - \tilde{G}_{\nu\mathbf{K}}^{-1}$ and the local interaction U. Calculating the Green's function $G_{\nu\mathbf{K}}^c$ using the cluster solver allows finding the next iteration for the cluster self-energy $\Sigma_{\nu\mathbf{K}}^c$, which closes the chain of self-consistent DCA equations.

As the cluster size increases, the DCA method provides faster convergence of results than the CDMFT: DCA corrections decrease quadratically as the cluster size increases, while the CMDFT ones decrease linearly [126]. We note, however, that, even for resource-demanding calculations with a 4×4 cluster, the achievement of practical convergence of the result with an increase in cluster size cannot be considered established in the DCA. Nevertheless, an important advantage of the DCA method is that calculations with it allow reliably obtaining superconductivity and a pseudogap in the two-dimensional Hubbard model [124, 125].

A further search for the best cluster method has led to the emergence of the *variational cluster approximation* (VCA) scheme [127–130]. In the VCA method, various cluster theories are considered from the standpoint of the Luttinger–Ward functionals that generate them. The optimum cluster scheme corresponds to the minimization of this functional. Figure 8 shows an example of calculating the antiferromagnetic and superconducting order parameters [130] with the VCA method for the two-dimensional Hubbard model.

Speaking about the disadvantages of cluster methods, we must first of all note the high computational complexity, which sharply increases with the increase in cluster size. In addition, in any case, cluster methods cannot describe the

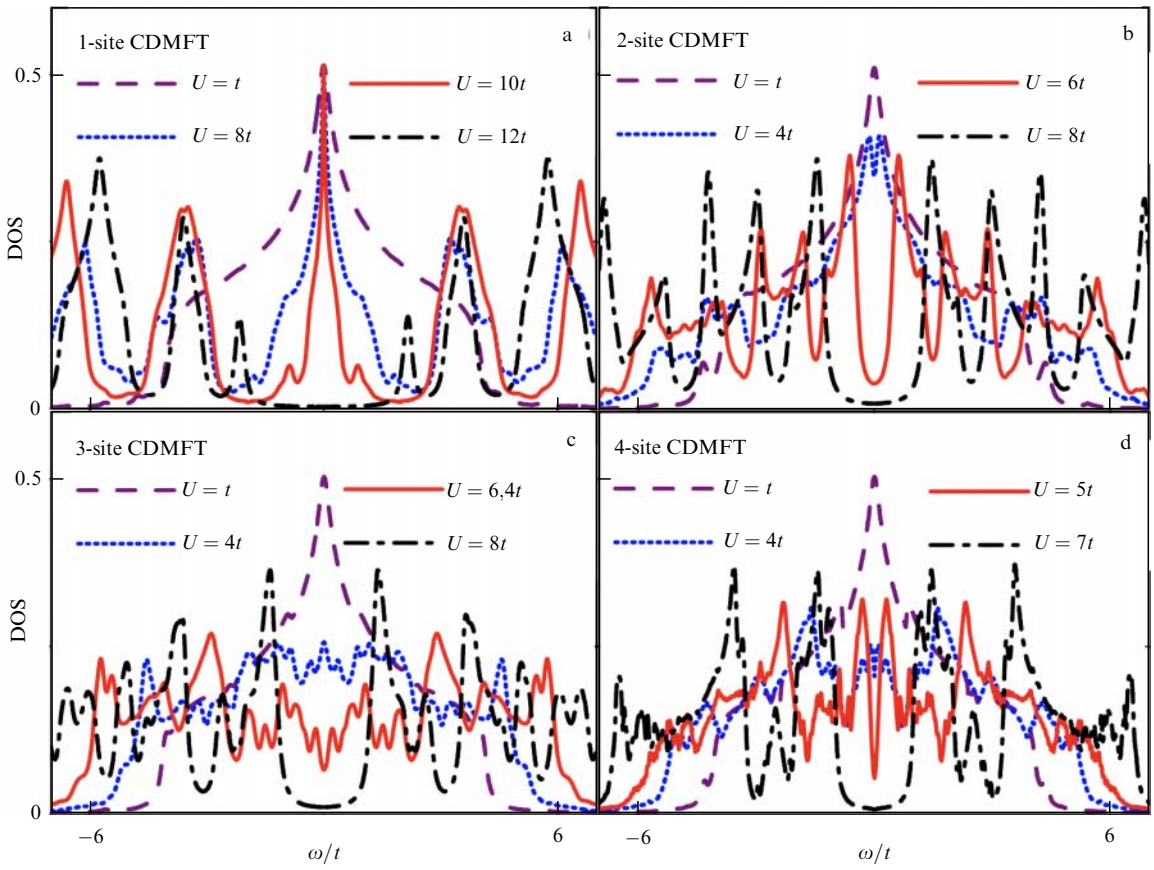

Figure 7. Density of states (DOS) as a function of the actual frequency ω calculated using the CDMFT for clusters ranging from 1 to 4 sites in size at different interaction strengths U. As the cluster size increases, a gap in the density of states opens at progressively lower U, which do not correspond to the Mott insulator state, possibly indicative of the existence of a pseudogap in the two-dimensional Hubbard model [120].

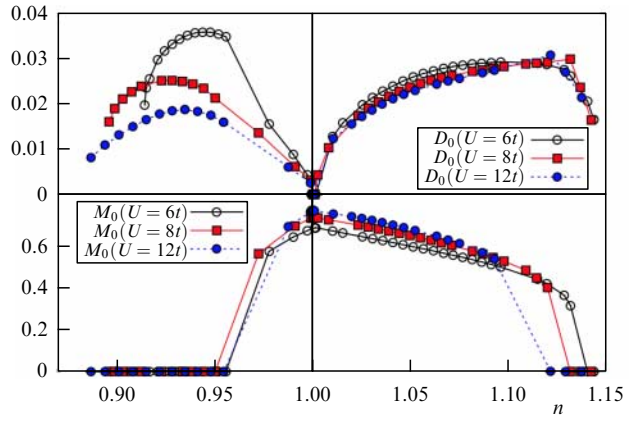

Figure 8. Dependences of order parameters for d-wave superconductivity (D_0) and antiferromagnetism (M_0) at zero temperature on electron density n for 2×4 clusters at $U = 6t$, $8t$, and $12t$ calculated using the VCA [130].

physics associated with the existence of long-wavelength collective fluctuations on scales exceeding several lattice constants. For a number of many-particle systems, including planar and layered (low-dimensional) ones, leading collective modes turn out to be highly delocalized, and their fluctuations can occur in a wide range of amplitudes. In such cases, taking only local fluctuations into account on the cluster scale turns out to be insufficient, and further development of the methods is needed. Going beyond the DMFT in different directions is possible. Recently, considerable attention has been devoted to the development of a family of diagram methods constructed on top of the result of a single-site DMFT scheme [131]. We review the main representatives of this family of methods in Section 4.

4. Post-DMFT methods

4.1 Accounting for nonlocal correlations using diagram methods

In the context of constructing post-DMFT theories, diagrams include strongly renormalized vertex functions that describe the local physics, and lines represent nonlocal effects. Various methods of this family differ from each other, usually in the way of renormalizing the vertex functions and/or in choosing the retained diagram types. This approach, unfortunately, has a number of disadvantages, significant among which is the rapidly growing complexity of practical calculations when introducing new expansion terms that are important for taking nonlocal correlations into account.

In Sections 4.1.1–4.1.3, we consider several diagram methods. We start with a description of the dual variable formalism as an illustration of the general approach to the construction of perturbative diagram theories and then proceed to specific implementations.

4.1.1 Methods of dual variables and the dynamical vertex approximation. We again consider the Hubbard action in

Eqn (26). Each term $\sum_{\nu\mathbf{k}\sigma} c^{\dagger}_{\nu\mathbf{k}\sigma}(\varepsilon_{\mathbf{k}} - \Delta_\nu)c_{\nu\mathbf{k}\sigma}$ in the partition function $\mathcal{Z} = \int \exp(-S)\mathcal{D}[c^{\dagger}, c]$ of that system can be subjected to the Hubbard–Stratonovich transformation [132, 133]

$$\exp\left[-c^{\dagger}(\varepsilon_{\mathbf{k}} - \Delta_\nu)c\right] = \mathcal{G}_\nu(\varepsilon_{\mathbf{k}} - \Delta_\nu) \times \int \exp\left\{-\left[\mathcal{G}_\nu^{-1}(f^{\dagger}c + c^{\dagger}f) + \mathcal{G}_\nu^{-2}(\varepsilon_{\mathbf{k}} - \Delta_\nu)^{-1}f^{\dagger}f\right]\right\}\mathcal{D}[f^{\dagger}, f]\,, \tag{33}$$

where c and $c^{\dagger}$ are Grassmann variables corresponding to a chosen mode $(\nu, \mathbf{k}, \sigma)$, and f and $f^{\dagger}$ are dual fermions (DFs) [134]. After this transformation in the partition function, we can formally integrate over the original variables $c^{\dagger}$ and c, with the result

$$\mathcal{Z} = Z_0 \int \exp\left\{-\sum_{\nu\mathbf{k}\sigma}\left(\mathcal{G}_\nu - (\varepsilon_{\mathbf{k}} - \Delta_\nu)^{-1}\right)\mathcal{G}_\nu^{-2} f^{\dagger}_{\nu\mathbf{k}\sigma} f_{\nu\mathbf{k}\sigma} - \sum_j V[f_j^{\dagger}, f_j]\right\}\mathcal{D}[f^{\dagger}, f]\,, \tag{34}$$

where Z_0 is a factor arising from the Hubbard–Stratonovich transformation; for the dual potential $V[f_j^{\dagger}, f_j]$, the Taylor expansion coefficients are known: they are given by the total vertex functions of the impurity problem. In the leading order, for instance, we have

$$V[f_j^{\dagger}, f_j] \approx -\sum_{\nu\nu'\Omega\sigma\sigma'} \gamma^{(2)}_{\nu\nu'\Omega,\sigma\sigma'} f^{\dagger}_{\nu i\sigma} f_{\nu+\Omega,i,\sigma} f^{\dagger}_{\nu'+\Omega,i,\sigma'} f_{\nu' i\sigma'}\,,$$

where $\gamma^{(2)}$ is the full two-particle vertex function of the Anderson impurity problem,

$$\gamma^{(2)}_{\nu\nu'\Omega} = \mathcal{G}_\nu^{-1}\mathcal{G}^{-1}_{\nu'+\Omega}\mathcal{G}^{-1}_{\nu'}\mathcal{G}^{-1}_{\nu+\Omega}\mathcal{G}^{(2)}_{\nu\nu'\Omega} - T^{-1}\mathcal{G}_\nu^{-1}\mathcal{G}^{-1}_{\nu'}\delta_{\Omega 0} + T^{-1}\mathcal{G}_\nu^{-1}\mathcal{G}^{-1}_{\nu+\Omega}\delta_{\nu\nu'}\,, \tag{35}$$

where $\mathcal{G}^{(2)}_{\nu\nu'\Omega} = \langle c^{\dagger}_{\nu\sigma} c_{\nu+\Omega,\sigma} c^{\dagger}_{\nu'+\Omega,\sigma'} c_{\nu'\sigma'}\rangle$ is the two-particle Green's function [83] in the Anderson impurity problem, $\langle\ldots\rangle = \mathcal{Z}^{-1}\int\ldots\exp(-\mathcal{S})D[c^{\dagger}, c]$ is the averaging over the impurity problem, and $\delta_{\nu\nu'}$ is the Kronecker symbol.

The advantage of switching to DFs is that, by appropriately choosing the hybridization Δ, one can take some of the correlations into account in the procedure of moving to the new variables and thus significantly suppress correlations in the dual system. This motivates constructing a diagram expansion about local theories in powers of $V[f_j^{\dagger}, f_j]$, expecting the expansion to have good convergence properties. For example, if we choose the DMFT hybridization to be Δ, then the zeroth order of the resulting theory reproduces the DMFT, the first-order correction vanishes, and the second-order correction allows reproducing significant effects of the physics of HTSC cuprates that are absent on the single-site DMFT level: the formation of arcs and pinning of the van Hove singularity on the Fermi surface [135].

By analogy with the DF method, one can construct a transition procedure to *dual bosons* (DBs) [136]. In the case of DBs, the diagram decomposition of the dual system is carried out around the *extended DMFT* (EDMFT) [111]. This approach works well in describing systems with pronounced collective (bosonic) modes. However, the *Firtz ambiguity*, which is characteristic of all bosonic methods of this kind, must be taken into account: the final result of calculations strongly depends on the specific method for dividing the fermion–fermion interaction into channels [137, 138].

Another possible generalization of the DMFT method is the *dynamical vertex approximation,* DΓA [139], based on the assumption of the locality of the full irreducible two-particle vertex function in the two-dimensional Hubbard model, which is confirmed by cluster computation data [140]. This approach allows using the Anderson impurity problem to calculate local vertex functions, which are then used to calculate one-particle and two-particle Green's functions of the full problem using parquet equations or ladder diagrams (see Section 4.1.3). The whole procedure is entirely analogous to the DMFT, but at the two-particle level: the self-consistency condition states the equality of the local part of the completely irreducible vertex function of the Hubbard model and the completely irreducible vertex function of the impurity problem. The set of diagrams generated by DΓA is quite close to the DF perturbative series, although there are some variations [141].

We also note a number of methods in which the single-particle Green's functions are subjected to the procedure to establish self-consistency. For example, in the DMFT + $\Sigma_{\mathbf{k}}$ approximation [142, 143], a characteristic spatial scale ξ associated with nonlocal fluctuations is introduced into the self-consistent DMFT equations. In turn, the DMFT + FLEX method [144], which includes loop and ladder diagrams, can be interpreted as a simplified version of the parquet equation method described in Section 4.1.3, in the sense that DMFT + FLEX allows considering fluctuations in different channels simultaneously.

One of the main advantages of the diagram methods mentioned above is the fundamental possibility of simultaneously taking local and nonlocal effects into account. But the practical applicability of these methods, unfortunately, is severely limited due to high computation costs entailed by their implementation. For example, the diagram series of the DF, DB, and DΓA methods include local four-point vertices, which requires calculating an object with four external frequency indices, and, in the case of multiorbital systems, also with orbital indices.

4.1.2 TRILEX and D-TRILEX methods. In 2015, an attempt was made to overcome the limitations on the range of nonlocal correlations without overstretching the method in terms of computation costs. In [145, 146], a diagram computational scheme, *TRILEX* (TRiply-Irreducible Local EXpansion), was proposed, based on the self-consistent approximation of the vertex function Λ that describes the fermion–boson interaction.

The first step in the TRILEX construction scheme is the separation of the interaction term into two channels, spin and charge, using the Hubbard–Stratonovich transformation. The auxiliary bosonic fields introduced in this way are coupled to the fermionic ones, which is described by the effective fermion–boson vertex Λ renormalized by the interaction. This quantity enters the expression for the self-energy function and the polarization operator via the Dyson equation

$$\Sigma_{\nu\mathbf{k}} = G^{-1}_{0,\nu\mathbf{k}} - G^{-1}_{\nu\mathbf{k}} = -\sum_{\Omega\mathbf{q}\eta} \lambda^{\eta} G_{\nu+\Omega,\mathbf{k}+\mathbf{q}} W^{\eta}_{\Omega\mathbf{q}} \Lambda^{\eta}_{\nu\Omega\mathbf{k}\mathbf{q}}\,, \tag{36}$$

$$P^{\eta}_{\Omega\mathbf{q}} = W^{-1}_{0,\Omega\mathbf{q}} - W^{-1}_{\Omega\mathbf{q}} = 2\sum_{\nu\mathbf{k}} \lambda^{\eta} G_{\nu+\Omega,\mathbf{k}+\mathbf{q}} G_{\nu\mathbf{k}} \Lambda^{\eta}_{\nu\Omega\mathbf{k}\mathbf{q}}\,, \tag{37}$$

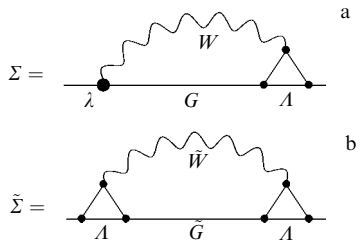

Figure 9. Diagram of the nonlocal self-energy function of (a) TRILEX and (b) D-TRILEX methods. G and W ($\tilde{G}$ and $\tilde{W}$) are fermionic and bosonic propagators in the direct (dual) space.

where G_0, W_0 and G, W are the lattice Green's functions of the fermionic and bosonic fields, respectively free and with interaction, and λ is the free fermion–boson vertex (Fig. 9a). The index η ranges in the values 0, x, y, z, with $\eta = 0$ corresponding to the charge channel and the other three values corresponding to the spin polarization components in the magnetic channel.

The Dyson equations are formally exact. The TRILEX approximation itself in its simplest form amounts to assuming the fermion–boson vertex function to be local and coincident with the vertex function of the impurity problem, the action for which has the form

$$\mathcal{S}_{\mathrm{f-b}}[c^{\dagger}, c, d] = -\sum_{\nu\mathbf{k}\sigma} c^{\dagger}_{\nu\mathbf{k}\sigma}\mathcal{G}^{-1}_{0,\,\nu\mathbf{k}\sigma}c_{\nu\mathbf{k}\sigma} - \frac{1}{2}\sum_{\Omega\mathbf{q}} d_{\Omega\mathbf{q}}\mathcal{W}'^{-1}_{\Omega\mathbf{q}}d_{-\Omega,-\mathbf{q}} + \sum_{\mathbf{kq}}\sum_{\nu\Omega}\sum_{\sigma\sigma'}\lambda_{\nu\Omega}c^{\dagger}_{\nu\mathbf{k}\sigma}\sigma^{\eta}_{\sigma\sigma'}c_{\nu+\Omega,\,\mathbf{k}+\mathbf{q},\,\sigma'}d_{-\Omega,-\mathbf{q}}\,. \tag{38}$$

The requirement that local functions coincide with those of the auxiliary impurity problem ($\sum_k G_{\nu\mathbf{k}} = \mathcal{G}_\nu$ and $\sum_k W_{\Omega\mathbf{k}} = \mathcal{W}_\Omega$) closes the TRILEX system of equations.

By construction, it is claimed that TRILEX, on the one hand, describes the local (Mott) physics, and, on the other hand, takes long-range correlations into account. This allows regarding TRILEX as a full-fledged alternative to the DMFT cluster versions. For example, as shown in [147, 148], single-site TRILEX is capable of describing d-wave superconductivity, which in terms of the DMFT is only possible in its cluster generalization. Good results can be obtained by applying the method to models where the spin–orbit coupling plays a significant role in the background of a strong local interaction [149]. Another important advantage of the TRILEX method is that, in contrast, for example, to the related GW + DMFT method [150–153], it takes both charge and spin fluctuations into account. However, as in other schemes based on the division of local interaction into channels, TRILEX suffers from the Firtz uncertainty problem. The current lack of a systematic strategy to resolve the Firtz uncertainty makes it impossible to apply the TRILEX method to the description of interacting fermionic systems in the regime of strong bosonic fluctuations in several channels or to the description of multiorbital systems, in particular, isotropic spin fluctuations in perovskite materials [154].

An attempt to overcome this obstacle was the cluster generalization of the TRILEX method [155]. In that case, the Firtz parameter, which determines the division of interaction into channels, is considered free, to be determined so as to ensure the best convergence of the numerical scheme. However, this does not free the cluster TRILEX method from the previously noted shortcomings of cluster generalizations of the DMFT, including translation symmetry breaking: the diagram of a nonlocal self-energy function within a cluster varies between neighboring clusters. It was also shown in [156] that the asymmetry of the TRILEX diagrams for self-energy and polarization functions leads to incorrect results for susceptibility in the strong-coupling regime.

The above problems were solved by the authors of a related method called *dual TRILEX* (D-TRILEX) [157, 158]. D-TRILEX is another diagram computational scheme based on partial bosonization (via the Hubbard–Stratonovich transformation) and starts with a transition to dual variables, which allows distinguishing among fermion–fermion, boson–boson, and fermion–boson interactions; as usual, the consideration is limited to the lowest order in the interaction of fermions and bosons,

$$\tilde{S}_{\mathrm{f-b}} = -\sum_{\nu\mathbf{k}\sigma} f^{\dagger}_{\nu\mathbf{k}\sigma}\tilde{G}^{-1}_{\nu\mathbf{k}\sigma}f_{\nu\mathbf{k}\sigma} - \frac{1}{2}\sum_{\Omega\mathbf{q}\eta} b^{\eta}_{\Omega\mathbf{q}}\tilde{W}^{\eta\,-1}_{\Omega\mathbf{q}}b^{\eta}_{-\Omega,-\mathbf{q}} + \sum_{\mathbf{kq}}\sum_{\nu\Omega}\sum_{\eta\sigma\sigma'}\Lambda^{\eta}_{\nu\Omega}f^{\dagger}_{\nu\mathbf{k}\sigma}\sigma^{\eta}_{\sigma\sigma'}f_{\nu+\Omega,\,\mathbf{k}+\mathbf{q},\,\sigma'}b^{\eta}_{-\Omega,-\mathbf{q}}\,, \tag{39}$$

where $f^{\dagger}$ and f are dual fermionic variables, b are dual bosonic variables, and $\tilde{W}$ is a dual bosonic propagator in the absence interaction. The boson–fermion vertex Λ of the impurity problem in this formalism is a nonrenormalized lattice-model vertex $\tilde{S}_{\mathrm{f-b}}$. The highest of the discarded terms in expansion (39) contain the four-point vertex $\gamma^{(2)}$ describing the fermion–fermion interaction, neglecting which simply turns out to be impossible. On the other hand, direct calculation of $\gamma^{(2)}$ is a rather resource-demanding computational problem. Therefore, the D-TRILEX formalism is constructed so as to select a specific type of bosonic interaction so as to minimize the contribution of the $\gamma^{(2)}$ vertex to the diagram series.

Next, the self-energy function and the polarization operator are determined by the leading (second) order of the expansion in Λ:

$$\tilde{\Sigma}_{\nu\mathbf{k}} = -\sum_{\Omega\mathbf{q}\eta}\Lambda^{\eta}_{\nu+\Omega,-\Omega}\tilde{G}_{\nu+\Omega,\,\mathbf{k}+\mathbf{q}}\tilde{W}^{\eta}_{\Omega\mathbf{q}}\Lambda^{\eta}_{\nu\Omega}\,, \tag{40}$$

$$\tilde{P}^{\eta}_{\Omega\mathbf{q}} = 2\sum_{\nu\mathbf{k}}\Lambda^{\eta}_{\nu+\Omega,-\Omega}\tilde{G}_{\nu+\Omega,\,\mathbf{k}+\mathbf{q}}\tilde{G}_{\nu\mathbf{k}}\Lambda^{\eta}_{\nu\Omega}\,. \tag{41}$$

We note that the Λ vertices enter the D-TRILEX expressions in a symmetric way, unlike those in similar expressions of the TRILEX method (cf. Figs 9a and b). A detailed discussion of the specifics of constructing such diagrams in dual variables is offered, for example, in [159]. An expansion of the full vertex function similar to that used in D-TRILEX can also be found in paper [160], published almost simultaneously with [157]. The authors of [160] called this approach the *single-boson exchange* (SBE) decomposition.

The D-TRILEX method is based in the approximation of the DB scheme, which means that this method inherits the self-consistency property from the parent scheme and does not therefore suffer from the Firtz ambiguity problem. The division into spin (s) and charge (c) channels is done for an artificially introduced coupling,

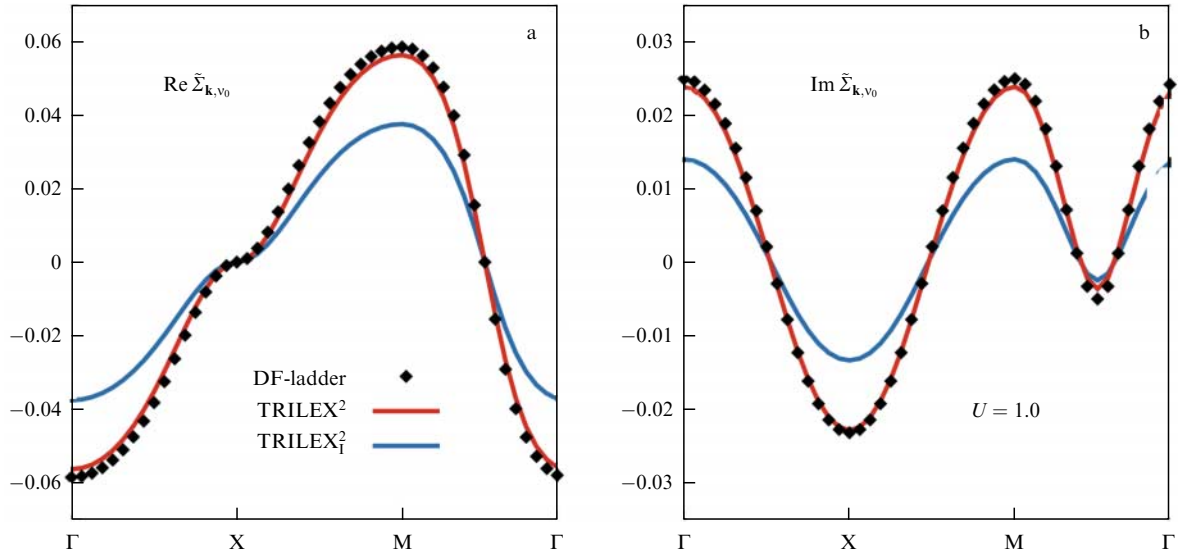

Figure 10. Comparison of results of calculations for the real and imaginary parts of the nonlocal component of the self-energy function at the first Matsubara frequency, obtained using the DF method (DF-ladder), D-TRILEX with the decomposition $U^\mathrm{c} = -U^\mathrm{s} = U/2$ (TRILEX^2), and D-TRILEX with the Ising decomposition of the coupling (TRILEX$_\mathrm{I}^2$) [157].

and the criterion for choosing a specific division type $U^\mathrm{c} = -U^\mathrm{s} = U/2$ is, as mentioned, the minimization of the contribution of diagrams discarded in accordance with the adopted approximation.

Among the advantages of D-TRILEX, we note the comparative ease and low computation costs of its implementation, which, notably, allows applying this method to the description of systems, such as indium selenide, with strong Coulomb correlations in the background of significant electron–phonon interaction [161]. Moreover, the method allows obtaining results of the same accuracy as, for example, the much more resource-demanding DF (Fig. 10). We also note that D-TRILEX is free from nonphysical divergences of the self-energy function that arise in a number of approaches using the inversion of the response function matrix [162–164].

D-TRILEX is a self-consistent diagram extension of the DMFT that takes collective electron fluctuations into account. Importantly, it can be successfully applied to the description of multiorbital systems [154]. At the time of writing, this method is the only one that allows describing nonlocal correlations in strongly interacting multiorbital systems. The authors of a series of papers [165–167] have developed a full-fledged multiband version of the D-TRILEX method and successfully applied it to describing the properties of the generalized Hubbard model on cubic and square lattices, the two-orbital Hubbard–Kanamori lattice, and a two-layer Hubbard lattice.

To summarize, we can characterize methods of the TRILEX type as an attempt to combine the exact description of local fluctuations using the DMFT and the approximate description of nonlocal effects at the level of the *GW* method. The principal point here is that nonlocal fluctuations are included into consideration without taking the mutual influence of the channels into account. However, this is known to be insufficient for a number of physical systems, including cuprates, because collective fluctuations occur there in several channels simultaneously and can influence each other. In Sections 4.1.3 and 4.2, we expound on the methods that allow taking the corresponding effects into account.

4.1.3 Method of parquet equations in dual variables and the functional renormalization group. A developed diagram approach to taking nonlocal correlations into account in all channels simultaneously is the *method of parquet equations*. It is based on the parquet decomposition of the full vertex function F into a completely irreducible vertex Λ and vertices Φ_r that are reducible in particle–hole, particle–hole transverse, and particle–particle scattering channels ($r = \mathrm{ph}, \overline{\mathrm{ph}}, \mathrm{pp}$). The term *completely irreducible* means that these diagrams cannot be divided into disconnected pieces by cutting any two lines. The reducible vertices Φ_r, in turn, can be cut along two internal lines (Fig. 11). Vertex functions Φ_r can be constructed from the corresponding irreducible vertices $\Gamma_r = F - \Phi_r$ using ladder equations, schematically written as $\Phi_r = FGG\Gamma_r$, also known as the *Bethe–Salpeter* (BS) *equa-*

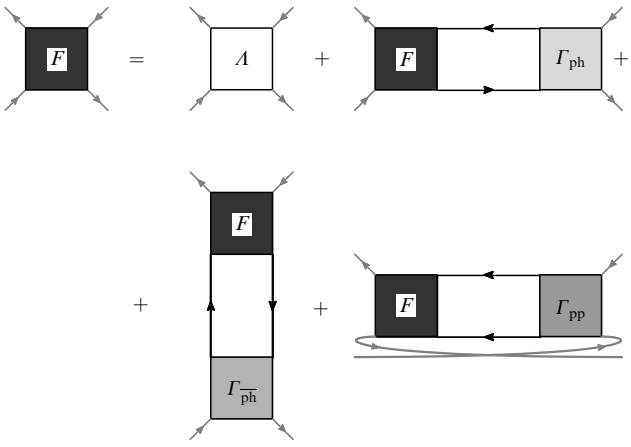

Figure 11. Parquet decomposition of full vertex function F into a completely irreducible vertex part Λ and reducible vertices Φ_ph, $\Phi_{\overline{\mathrm{ph}}}$, and Φ_pp. Reducible vertices Φ_r are expressed in terms of irreducible vertices $\Gamma_r = F - \Phi_r$ using Bethe–Salpeter equations.

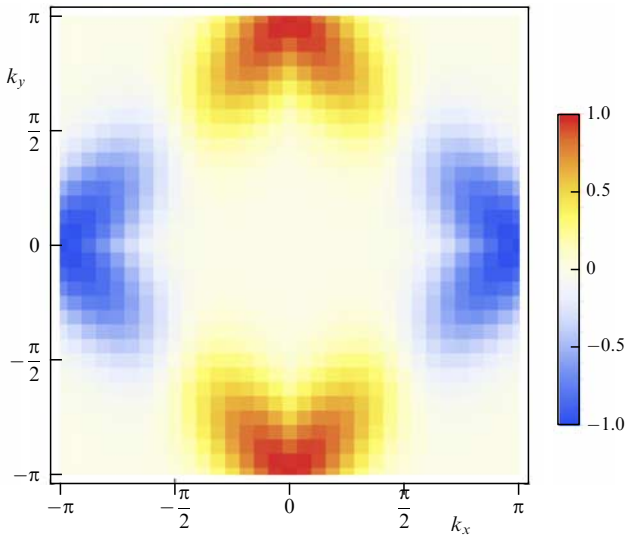

Figure 12. Eigenfunction corresponding to largest eigenvalue $\lambda_{pp} = 0.99$ of the Bethe–Salpeter equations calculated on a 32×32 lattice by the method of parquet equations in dual variables. Form of the function indicates the presence of d-wave superconductivity in the doped two-dimensional Hubbard model [174].

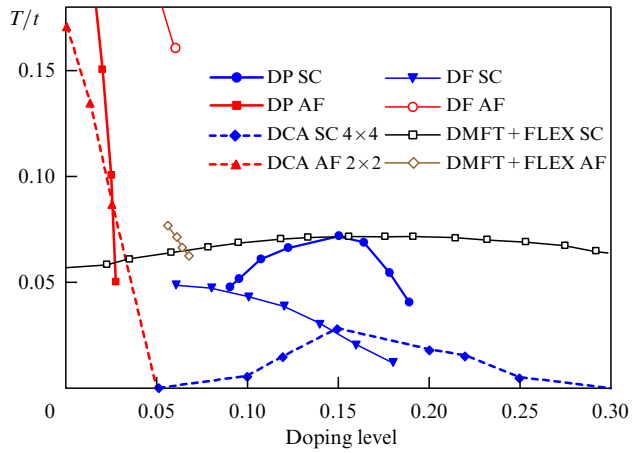

Figure 13. Phase diagram of the two-dimensional Hubbard model in coordinates (doping level, temperature) obtained using various methods: dual parquet (DP) equations for $U = 8t$, $t' = -0.2t, t'' = 0.1t$, DCA for $U = 6t$, $t' = -0.2t$, and $t'' = 0$, DF in the ladder approximation for $U = 8t$, $t' = t'' = 0$, DMFT + FLEX method for $U = 5t$, $t' = -0.2t$, and $t'' = 0.16t$. Here, t, t', and t'' are the respectively amplitudes of hops between nearest sites, along the diagonal, and over a site. Blue curves correspond to the transition to the superconducting state, and red curves, to antiferromagnetic ordering [174].

tion. Supplemented with the Schwinger–Dyson equation relating the self-energy Σ to the full vertex F, the parquet and BS equations form a closed system and are solved self-consistently. For a detailed acquaintance with the method of parquet equations, we refer the reader to the classic survey [168], as well as to recent work where the method of parquet equations, free of any approximation, was first applied to small Hubbard clusters [169, 170].

The main advantages of the method of parquet equations include taking all effects into account based on the mutual screening of various bosonic modes. In the framework of this approach, it is possible to construct all one- and two-particle correlation functions given the full irreducible vertex function. However, although various approximations of this full function are used in practical implementations, the method of parquet equations entails high computation costs. This restricts the size of physical systems amenable to the description: the maximum size of the momentum lattice is currently 6×6 sites [171, 172].

We note the achievements of recent years in the field of numerically solving the parquet equations. First, the use of the high-frequency asymptotic form of the Green's functions [170] and the form-factor basis for the spatial indices of the vertex functions [172] have allowed using smaller frequency and momentum lattices with greater efficiency. Second, the method of partial bosonization of the vertex functions for parquet equations was implemented in [173], allowing the long-wavelength fluctuations to be described as bosonic degrees of freedom. The computational advantage is achieved by switching from four-point to three-point Green's functions.

A significant reduction in the numerical complexity of solving parquet equations was possible by moving to dual variables, as in [174]. With this procedure, the high-energy physics associated with local correlations is taken into account at the level of the transition to dual variables, such that the parquet equations actually describe only low-energy processes associated with fluctuations in the collective modes of the system. This allows integrating out most of the Matsubara frequencies, restricting oneself to lower-order diagrams. The low-energy model constructed in this way, which includes only the lower Matsubara frequencies, allows an efficient solution for lattices with up to 32×32 sites (Fig. 12), with all fluctuations in different channels taken into account on an equal footing.

Accounting for nonlocal correlations in several channels is of fundamental importance, for example, when describing systems with quantum phase transitions or when considering scenarios of Cooper pairing due to spin fluctuations. Figure 13 shows the phase diagram of a two-dimensional Hubbard lattice for parameters corresponding to HTSC cuprates. As we can see, taking the mutual influence of bosonic modes into account at the level of the single-site DMFT or the ladder-approximation DF constructed on top of it does not reproduce the typical dome-shaped structure of the superconducting phase, and the cluster method (DCA), which is very expensive in terms of numerical resources, reproduces it less pronouncedly than the dual parquet formalism. This can be explained by the absence in DCA of the necessary renormalizations of the two-particle vertex function in the long-wavelength range.

The functional renormalization group (fRG) method [177, 178] can also be used to describe systems with competing instabilities. The idea of the original method is a smooth evolution to a correlated system from an exactly solvable Gaussian system. Such an evolution generates equations containing correlation functions that are typically cut off at the two-particle level. This technique works successfully for weak interparticle interaction, but in the strong-coupling regime it requires higher-loop corrections to be taken into account. A number of papers [179–181] show the equivalence of the multiloop fRG method and parquet equations; the methods also show comparable computational complexity.

The fRG equations can also be generalized to the case where the starting point of the renormalization group flow is a collection of isolated Anderson impurity problems with parameters corresponding to the DMFT solution [175]. The

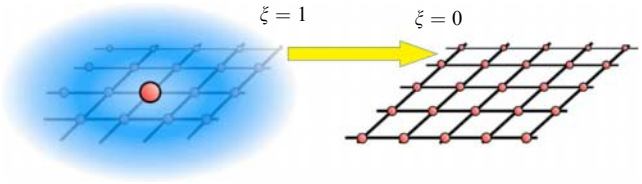

Figure 14. Illustration of the DMF^{2}RG method, which consists of the evolution from the impurity Anderson problem ($\xi = 1$) to the full lattice problem ($\xi = 0$) via renormalization group equations [175].

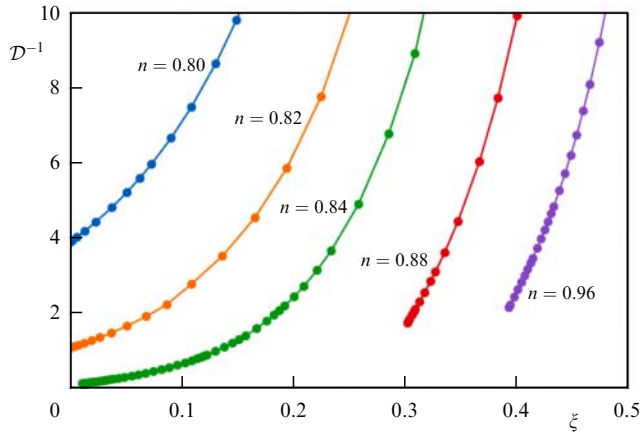

Figure 15. Dependence of inverse effective coupling $\mathcal{D}$ in the Cooper d-wave channel on parameter ξ at different values of electron density n, obtained using the DMF^{2}RG method for the Hubbard model with parameters $U = 8t$, $t' = -0.2t$, and $T = 0.08t$. $\xi = 1$ corresponds to a collection of impurity problems, and $\xi = 0$, to the Hubbard model [176].

action can then be written as

$$\mathcal{S}^{\xi} = \sum_{\nu\mathbf{k}\sigma} \left(\mathrm{i}\nu - \xi\Lambda_\nu - (1-\xi)\varepsilon_{\mathbf{k}}\right) c^{\dagger}_{\nu\mathbf{k}\sigma} c_{\nu\mathbf{k}\sigma} + \sum_i \int_0^{1/T} \mathrm{d}\tau\, U n_{\tau i\uparrow} n_{\tau i\downarrow}\,, \tag{42}$$

where the free term is determined by the contribution of both the Anderson impurity problem and the noninteracting lattice problem. The starting point $\mathcal{S}^{\xi=1}$ corresponds to a collection of identical impurity problems whose hybridizations are obtained from the DMFT, and $\mathcal{S}^{\xi=0}$ corresponds to the Hubbard model (Fig. 14).

Similarly to other schemes that take the mutual influence of various fluctuation channels into account, the fRG method also signals the presence of a superconducting dome in the phase diagram of the Hubbard model. Figure 15 shows the dependence, obtained in [176] for different electron densities, of the inverse effective coupling for the d-wave pairing of electrons corresponding to the wave vector $\mathbf{Q} = 0$ and zero frequency on the renormalization group flow parameter ξ. For density $n = 0.96$ and $n = 0.88$, the flux is shown up to the critical values ξ_c at which magnetic instability occurs. It can be seen that, in approaching half filling from $n = 0.80$, the pairing correlations start increasing but cannot fully develop due to the appearance of magnetic instability.

4.2 Description of nonlocal correlations without the use of diagram series

The DMFT diagram expansions described in Section 4.1 allow consistently incorporating both local correlations and essentially nonlocal effects associated with the formation of collective modes. A numerically exact solution of the DMFT problem means that the theory does not contain constraints on the magnitude and nature of local correlations. However, it is easy to understand that summing up only the selected classes of diagrams implies certain assumptions about the nature of fluctuations. Namely, the use of ladder and parquet approximations is justified if the collective fluctuations can be considered Gaussian or nearly Gaussian. But this is not true, in particular, for finite systems (for example, magnetic molecules [182]) at sufficiently low temperatures. In that case, the collective degree of freedom corresponding to the order parameter is affected by a Mexican-hat potential, and hence the fluctuation statistics turn out to be essentially non-Gaussian. We next describe the fluctuating local field method that allows going beyond the local DMFT physics by introducing an auxiliary classical field without assumptions about the magnitude and nature of collective fluctuations.

4.2.1 Fluctuating local field method. As a new way of taking collective fluctuations into account, the *fluctuating local field* (FLF) method was proposed in [183]. Originally formulated to describe fluctuations of a classical field defined on a finite lattice, the method was subsequently generalized to quantum systems.

Assuming that the leading fluctuation channel is known, the FLF method is technically based on the exact transformation of the partition function, which for the lattice model described by an action S is expressed as

$$Z = \int \exp\left(-S[c^{\dagger}, c]\right) D[c^{\dagger}, c] = \left(\frac{N}{2\pi\varkappa T}\right)^{3/2} \times \iint \exp\left\{-S[c^{\dagger}, c] - \frac{N}{2T}\left(\varkappa||\bar{s}||^2 - 2(\zeta\bar{s}) + \frac{1}{\varkappa}||\zeta||^2\right)\right\} \times \mathcal{D}[c^{\dagger}, c]\, \mathrm{d}^3\zeta\,. \tag{43}$$

Here, ζ is an artificially introduced classical vector field conjugate to the order parameter $\bar{s}$, and $||\ldots||$ is the length of a vector. In the case of antiferromagnetic fluctuations, for example, the components of $\bar{s}$ are given by

$$\bar{s}^{\eta} = \frac{T}{N}\int_0^{1/T} \sum_j \exp\left[\mathrm{i}(\mathbf{q}\mathbf{r}_j)\right] c^{\dagger}_{\tau j\sigma} \sigma^{\eta}_{\sigma\sigma'} c_{\tau j\sigma'}\, \mathrm{d}\tau\,,$$

where $\mathbf{q} = (\pi, \pi)$, $\mathbf{r}_j$ is the position of site j, and $\varkappa$ is a free parameter of the model that determines the amplitude of the ζ field fluctuations. We see that a full square is added to the exponent, such that the integration over ζ does indeed produce the original partition function. It is important to note that, if we first integrate over fermionic fields, then such a transformation can be regarded as the introduction of an ensemble $Z \propto \int Z_\zeta\, \mathrm{d}^3\zeta$, where Z_ζ is the partition function of the system at a specific value of the fluctuating field ζ. Calculating Z_ζ may be easier than the original Z because, due to the appearance of the $\varkappa\bar{s}^2$ term in the action for Z_ζ, order parameter fluctuations at each fixed value of ζ decrease compared to the original ones. This allows invoking the perturbation theory, which would be inapplicable for the original system. Convergence can be additionally improved by the optimal choice of $\varkappa$. The total magnitude of fluctuations is restored in that case by the subsequent integration over $\mathrm{d}\zeta$. Importantly, the proposed method does not impose restrictions on the magnitude and statistics of the moments of

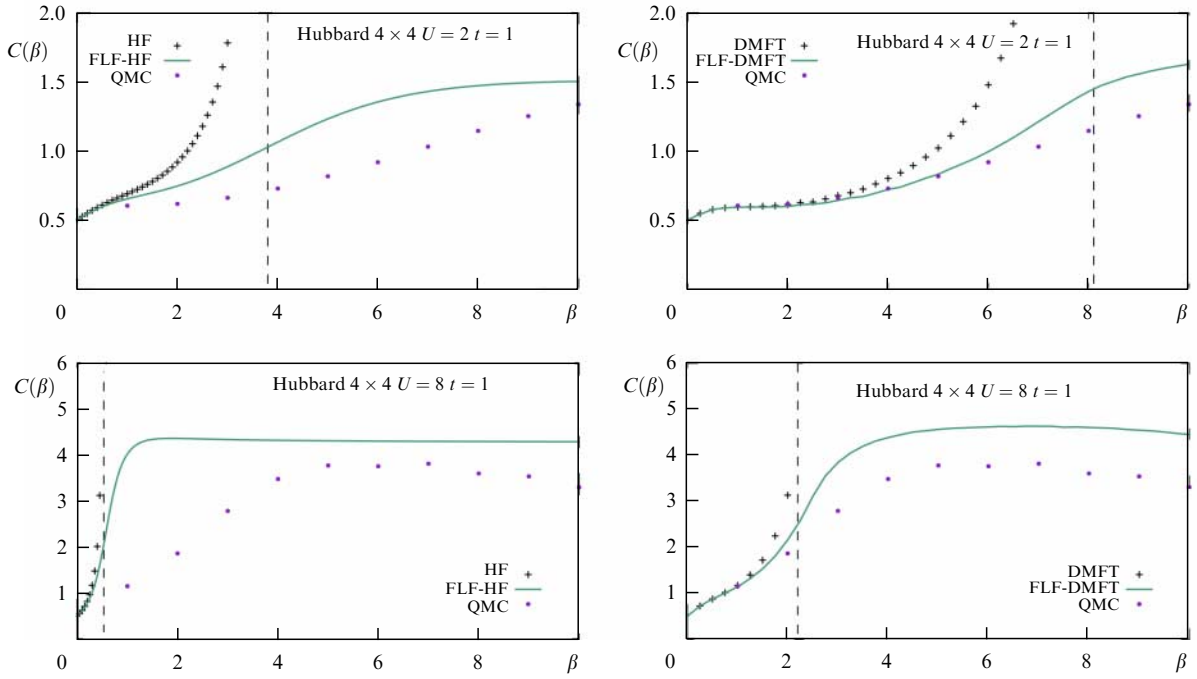

Figure 16. Calculated dependence of Curie constant C on inverse temperature $\beta = 1/T$ for a half-filled antiferromagnetic two-dimensional Hubbard lattice, obtained using the quantum Monte Carlo method (QMC), MF approximation (Hartree–Fock, HF), dynamical mean-field theory (DMFT), and fluctuating local field method based on them (FLF–HF and FLF–DMFT) [184].

the fluctuations under consideration: they can be essentially non-Gaussian.

In practice, the FLF method is developed based on some 'parent' approximation, such as the mean field or DMFT. Notably, the DMFT + FLF scheme was developed in [184] to describe nonlocal magnetic fluctuations in two-dimensional Hubbard clusters. According to the Mermin–Wagner theorem, this system is paramagnetic, and hence the DMFT solution in the absence of an external magnetic field should be based on the assumption of a zero local magnetic moment of the impurity. However, this approach does not include fluctuations of the impurity magnetic moment near the mean value, which are correlated across different lattice sites. In the FLF framework, this can be rectified by introducing the dependence of the impurity Green's function on the magnitude of the fluctuating field. In the simplest case, this dependence is linear; the impurity Green's function is expressed as

$$\mathcal{G}_\zeta^{\mathrm{FLF}} = \mathcal{G}_\zeta - \sum_\eta \zeta^\eta f_\zeta(\omega)\sigma^\eta_{\sigma\sigma'} \exp\left[\mathrm{i}(\mathbf{q}\mathbf{r}_j)\right], \tag{44}$$

where $\mathcal{G}_\zeta$ is the impurity Green's function corresponding to some hybridization Δ_ζ, calculated by the DMFT method under the assumption of no magnetic polarization, and $f_\zeta(\omega)$ determines the frequency profile of the ζ field. Thus, various values of the local magnetic moment are included in the consideration. Because the fluctuating field breaks the symmetry of the system, we use tensor notation in what follows. We introduce a tensor L whose nonzero components in the Fourier representation are $L^\eta_{\zeta,\mathbf{k},\mathbf{k}+\mathbf{q},\sigma,\sigma'} = f_\zeta(\omega)\sigma^\eta_{\sigma\sigma'}\exp[\mathrm{i}(\mathbf{q}\mathbf{r}_j)]$, such that expression (44) takes the form $\mathcal{G}_\zeta - (\zeta L)$ in tensor notation. Then, by analogy with the derivation of formula (29) for a Hubbard lattice with the dispersion $\varepsilon_\mathbf{k}$, we can obtain the free energy $F_\zeta = -T\ln Z_\zeta$ in the form [184]

$$F_\zeta = N\mathcal{F} - \ln\det\left[1 + \left(\mathcal{G} - (\zeta L)\right)(\Delta - \varepsilon)\right] + \frac{N}{2\varkappa}\zeta^2, \tag{45}$$

where $\mathcal{F}$ is the free energy of the unpolarized impurity, and the Green's function at a certain value of ζ is equal to $G_\zeta = [(\mathcal{G}_\zeta - (\zeta L))^{-1} + \Delta - \varepsilon]^{-1}$. The final DMFT-based FLF Green's function is obtained by averaging over all values of ζ,

$$G^{\mathrm{FLF}} = \left\langle \frac{1}{\left(\mathcal{G}_\zeta - (\zeta L)\right)^{-1} + \Delta - \varepsilon} \right\rangle_{\mathrm{FLF}}, \tag{46}$$

where $\langle\ldots\rangle_{\mathrm{FLF}} = Z^{-1}\int\ldots Z_\zeta\,\mathrm{d}^3\zeta$.

Finally, the value of the parameter $\varkappa$ and the function $f_\zeta(\omega)$ must be determined. This can be done by noting that fluctuations of the order parameter taken into account in the FLF method can be eliminated by replacing the averaging over ζ with the choice of a single value corresponding to the point ζ_0 at which Z_ζ is maximum (a saddle point). We require such an estimate to reproduce the result of the approach that is originally free of order parameter fluctuations, the DMFT. We consider the case of a system placed in a weak external field, which guarantees a deviation of ζ_0 from zero and the presence of spin polarization in the DMFT solution. We let G^{DMFT} denote the Green's function of such a spin-polarized solution. To determine $\varkappa$ and $f_\zeta(\omega)$, in accordance with our strategy, we then require that

$$G^{\mathrm{DMFT}} = \frac{1}{\left(\mathcal{G}_\zeta - (\zeta_0 L)\right)^{-1} + \Delta - \varepsilon}. \tag{47}$$

Condition (47) closes the system of FLF equations.

Figure 16 shows the results of calculations of the Curie constant $C = T\chi$, where χ is the susceptibility in the anti-

ferromagnetic channel, for half-filled 4×4 Hubbard lattices with $U = 2t$ (moderately correlated system) and $U = 8t$ (strongly correlated system) obtained using the FLF–HF (FLF based on the MF Hartree–Fock approximation) and FLF–DMFT schemes. The behavior of the system under study is determined, first, by the physics associated with the formation of local moments, and, second, by the developed collective antiferromagnetic fluctuations. Among the considered approximations, only FLF–DMFT includes both these mechanisms. It can be seen that this scheme also gives the best description of the Curie temperature constant.

We emphasize that the FLF method allows improving the accuracy of the results by increasing the number of considered oscillating modes near the leading one. The efficiency of the multimode FLF regime for the classical Ising and Heisenberg systems was demonstrated in [183]; in [185], this scheme was successfully used to calculate the free energy of one-dimensional Hubbard chains. We note, however, that an increase in the number of modes requires additional computation expenditures, and hence the FLF is currently technically limited in this respect. Nevertheless, the simplicity of the implementation, the flexibility of the method, and the absence of restrictions on the magnitude of collective fluctuations allow the FLF to be regarded as a promising numerical scheme for studying correlated systems in various modes. We also note that, although at the time of writing the method has been developed only for problems with one fluctuation channel, its construction scheme does not impose restrictions on the number of channels.

5. Conclusions

We have given a brief review of the numerical methods that exist today for describing correlated systems. Starting with the MF approximation, which maps a many-particle problem to a one-particle problem in an effective external field and does not take correlation effects into account, we first moved to a locally exact DMFT and then considered a number of schemes developed for taking nonlocal correlations into account.

In view of the significant achievements of the DMFT method, it is easy to understand why many subsequent frameworks use it as a basis. Accounting for nonlocal effects in the form of expansions near the local physics looks quite natural. However, we must not forget that a good numerical method must satisfy a number of requirements, one being that physical laws (symmetry, observable results, etc.) be taken into account. A simple software implementation and, whenever possible, low computation costs are also highly desirable. At the same time, describing phase transitions also implies the possibility of treating physical systems in a wide range of parameter values. Among the methods mentioned in this review, D-TRILEX and FLF satisfy these requirements, although this can be stated with full certainty only after a number of additional checks.

The physics of correlated multiparticle systems is being actively developed. In this review, we did not attempt anything close to covering all work in this field, or even presenting a complete list of the existing methods. However, we hope that our review will help the reader navigate across the landscape of post-DMFT schemes, and the list of references will enable those interested to gain deeper insights into particular methods. A good addition to this review is given by [186], where results of various schemes for a particular system (the half-filled Hubbard model with $U = 2t$) are systematically compared.

Acknowledgments

This study was supported by the Roadmap for the Development of the High-Technology Field "Quantum Computations" no. 1/17654-D dated July 10, 2019 (State Atomic Energy Corporation Rosatom). The work of Ya S L was supported by the National Research Nuclear University MEPhI under the Priority-2030 program.

References

1. Mott N F *Proc. Phys. Soc. A* **62** 416 (1949)
2. Roth L M *J. Phys. Chem. Solids* **23** 433 (1962)
3. Hubbard J *Proc. R. Soc. Lond. A* **276** 238 (1963)
4. Hubbard J *Proc. R. Soc. Lond. A* **277** 237 (1964)
5. Hubbard J *Proc. R. Soc. Lond. A* **281** 401 (1964)
6. Izyumov Yu A *Phys. Usp.* **38** 385 (1995); *Usp. Fiz. Nauk* **165** 403 (1995)
7. van Loon E G C P, Katsnelson M I *J. Phys. Conf. Ser.* **1136** 012006 (2018)
8. Bünemann J et al. *J. Phys. Condens. Matter* **19** 326217 (2007)
9. Aryasetiawan F et al. *Phys. Rev. B* **70** 195104 (2004)
10. Bednorz J G, Müller K A *Z. Phys. B* **64** 189 (1986)
11. Bardeen J, Cooper L N, Schrieffer J R *Phys. Rev.* **108** 1175 (1957)
12. Damascelli A, Hussain Z, Shen Z-X *Rev. Mod. Phys.* **75** 473 (2003)
13. Reznik D et al. *Nature* **440** 1170 (2006)
14. Lanzara A et al. *Nature* **412** 510 (2001)
15. Mackenzie A P, Maeno Y *Rev. Mod. Phys.* **75** 657 (2003)
16. Kamihara Y et al. *J. Am. Chem. Soc.* **130** 3296 (2008)
17. Petrovic C et al. *J. Phys. Condens. Matter* **13** L337 (2001)
18. Stewart S R *Rev. Mod. Phys.* **56** 755 (1984)
19. Lee P A, Nagaosa N, Wen X-G *Rev. Mod. Phys.* **78** 17 (2006)
20. Yan S, Huse D A, White S R *Science* **332** 1173 (2011)
21. Norman M R *Rev. Mod. Phys.* **88** 041002 (2016)
22. Izyumov Yu A, Kurmaev E Z *Phys. Usp.* **51** 23 (2008); *Usp. Fiz. Nauk* **178** 25 (2008)
23. Bakr W S et al. *Nature* **462** 74 (2009)
24. Mazurenko A et al. *Nature* **545** 462 (2017)
25. Geim A K, Grigorieva I V *Nature* **499** 419 (2013)
26. Yankowitz M et al. *Science* **363** 1059 (2019)
27. Balents L et al. *Nat. Phys.* **16** 725 (2020)
28. Kennes D M et al. *Nat. Phys.* **17** 155 (2021)
29. Christos M, Sachdev S, Scheurer M S *Phys. Rev. X* **12** 021018 (2022)
30. Song Z-D, Bernevig B A *Phys. Rev. Lett.* **129** 047601 (2022)
31. Weinberg P, Bukov M *SciPost Phys.* **2** 003 (2017)
32. Weinberg P, Bukov M *SciPost Phys.* **7** 020 (2019)
33. Liu X-Y, Qi C *Comput. Phys. Commun.* **259** 107349 (2021)
34. Amaricci A et al. *Comput. Phys. Commun.* **273** 108261 (2022)
35. Yoshimi K, Tsumuraya T, Misawa T *Phys. Rev. Res.* **3** 043224 (2021)
36. Ochi M, Koshino M, Kuroki K *Phys. Rev. B* **98** 081102 (2018)
37. Repellin C et al. *Phys. Rev. Lett.* **124** 187601 (2020)
38. Xie F et al. *Phys. Rev. B* **103** 205416 (2021)
39. Potasz P, Xie M, MacDonald A H *Phys. Rev. Lett.* **127** 147203 (2021)
40. Austin B M, Zubarev D Y, Lester W A (Jr.) *Chem. Rev.* **112** 263 (2012)
41. Needs R J et al. *J. Chem. Phys.* **152** 154106 (2020)
42. Foulkes W M C et al. *Rev. Mod. Phys.* **73** 33 (2001)
43. Burovski E A et al. *Phys. Rev. Lett.* **87** 186402 (2001)
44. Wagner L K, Ceperley D M *Rep. Prog. Phys.* **79** 094501 (2016)
45. Nakano K et al. *Phys. Rev. B* **103** L121110 (2021)
46. Becca F, Sorella S *Quantum Monte Carlo Approaches for Correlated Systems* (Cambridge: Cambridge Univ. Press, 2017)
47. Li Z-X, Yao H *Annu. Rev. Condens. Matter Phys.* **10** 337 (2019)
48. Hangleiter D et al. *Sci. Adv.* **6** eabb8341 (2020)
49. Huggins W J et al. *Nature* **603** 416 (2022)

50. Huang E W et al. *npj Quantum Mater.* **3** 22 (2018)
51. Jiang H-C, Devereaux T P *Science* **365** 1424 (2019)
52. Bollmark G, Laflorencie N, Kantian A *Phys. Rev. B* **102** 195145 (2020)
53. Bollmark G et al. *Phys. Rev. X* **13** 011039 (2023)
54. Schollwöck U *Rev. Mod. Phys.* **77** 259 (2005)
55. Schollwöck U *Ann. Physics* **326** (1) 96 (2011)
56. Baiardi A, Reiher M *J. Chem. Phys.* **152** 040903 (2020)
57. Jiang Y-F et al. *Phys. Rev. Res.* **2** 033073 (2020)
58. Peng C et al. *New J. Phys.* **23** 123004 (2021)
59. Mai P et al. *Proc. Natl. Acad. Sci. USA* **119** e2112806119 (2022)
60. Stemmle C, Paulus B, Legeza Ö *Phys. Rev. A* **97** 022505 (2018)
61. Beran P et al. *J. Chem. Theory Comput.* **17** 7575 (2021)
62. Sugihara T *J. High Energy Phys.* **2004** 007 (2004)
63. Stoudenmire E M, White S R *Annu. Rev. Condens. Matter Phys.* **3** 111 (2012)
64. Li Q et al. *Phys. Rev. Lett.* **130** 226502 (2023)
65. Tazhigulov R N et al. *PRX Quantum* **3** 040318 (2022)
66. Stair N H, Evangelista F A *PRX Quantum* **2** 030301 (2021)
67. Bravyi S B, Kitaev A Yu *Ann. Physics* **298** 210 (2002)
68. Seeley J T, Richard M J, Love P J *J. Chem. Phys.* **137** 224109 (2012)
69. Tranter A et al. *J. Chem. Theory Comput.* **14** 5617 (2018)
70. Gutzwiller M C *Phys. Rev. Lett.* **10** 159 (1963)
71. Predescu C *Phys. Rev. E* **66** 066133 (2002)
72. Feynman R P *Statistical Mechanics* (Reading, MA: W.A. Benjamin, 1972)
73. Stoner E C *Proc. R. Soc. Lond. A* **165** 372 (1938)
74. Becke A D *J. Chem. Phys.* **140** 18A301 (2014)
75. Jones R O *Rev. Mod. Phys.* **87** 897 (2015)
76. Hasnip P J et al. *Philos. Trans. R. Soc. A* **372** 20130270 (2014)
77. Zhang T et al. *RSC Adv.* **5** 106877 (2015)
78. Hohenberg P, Kohn W *Phys. Rev.* **136** B864 (1964)
79. Hybertsen M S, Schlüter M, Christensen N E *Phys. Rev. B* **39** 9028 (1989)
80. McMahan A K, Annett J F, Martin R M *Phys. Rev. B* **42** 6268 (1990)
81. Gunnarsson O, Schönhammer K *Phys. Rev. Lett.* **56** 1968 (1986)
82. Abrikosov A A, Gorkov L P, Dzyaloshinski I E *Methods of Quantum Field Theory in Statistical Physics* (New York: Dover Publ., 1975); Translated from Russian: *Metody Kvantovoi Teorii Polya v Statisticheskoi Fizike* (Moscow: Ripol Klassik, 2013)
83. Mahan G D *Many-Particle Physics* (Berlin: Springer, 2013)
84. Coleman P *Introduction to Many-Body Physics* (New York: Cambridge Univ. Press, 2015)
85. Nelson W et al. *Phys. Rev. A* **75** 032505 (2007)
86. Romaniello P, Guyot S, Reining L *J. Chem. Phys.* **131** 154111 (2009)
87. Schmidt P S, Patrick C E, Thygesen K S *Phys. Rev. B* **96** 205206 (2017)
88. Pavlyukh Y, Stefanucci G, van Leeuwen R *Phys. Rev. B* **102** 045121 (2020)
89. van Schilfgaarde M, Kotani T, Faleev S *Phys. Rev. Lett.* **96** 226402 (2006)
90. Anisimov V I, Aryasetiawan F, Lichtenstein A *J. Phys. Condens. Matter* **9** 767 (1997)
91. Metzner W, Vollhardt D *Phys. Rev. Lett.* **62** 324 (1989)
92. Yonezawa F, Morigaki K *Prog. Theor. Phys. Suppl.* **53** 1 (1973)
93. Altland A, Simons B D *Condensed Matter Field Theory* (Cambridge: Cambridge Univ. Press, 2010)
94. Anderson P W *Phys. Rev.* **109** 1492 (1958)
95. Elliott R J, Krumhansl J A, Leath P L *Rev. Mod. Phys.* **46** 465 (1974)
96. Rubtsov A N, Savkin V V, Lichtenstein A I *Phys. Rev. B* **72** 035122 (2005)
97. Werner P, Millis A J *Phys. Rev. B* **74** 155107 (2006)
98. Gull E et al. *Rev. Mod. Phys.* **83** 349 (2011)
99. Zingl M et al. *Physica B* **536** 254 (2018)
100. de Souza Melo B M et al. *J. Phys. Condens. Matter* **32** 095602 (2020)
101. Loh E Y (Jr.) et al. *Phys. Rev. B* **41** 9301 (1990)
102. Cohen G et al. *Phys. Rev. Lett.* **115** 266802 (2015)
103. Jarrell M, Gubernatis J E *Phys. Rep.* **269** 133 (1996)
104. Vidberg H J, Serene J W *J. Low Temp. Phys.* **29** 179 (1977)
105. Logan D E, Galpin M R *J. Phys. Condens. Matter* **28** 025601 (2016)
106. Park H, Haule K, Kotliar G *Phys. Rev. Lett.* **101** 186403 (2008)
107. Sun P, Kotliar G *Phys. Rev. B* **66** 085120 (2002)
108. Biermann S, Aryasetiawan F, Georges A *Phys. Rev. Lett.* **90** 086402 (2003)
109. Ayral T, Biermann S, Werner P *Phys. Rev. B* **87** 125149 (2013)
110. Kotliar G et al. *Rev. Mod. Phys.* **78** 865 (2006)
111. Georges A et al. *Rev. Mod. Phys.* **68** 13 (1996)
112. Held K et al. *Phys. Rev. Lett.* **86** 5345 (2001)
113. McWhan D B, Rice T M, Remeika J P *Phys. Rev. Lett.* **23** 1384 (1969)
114. Zang J et al. *Phys. Rev. X* **12** 021064 (2022)
115. Maier T et al. *Rev. Mod. Phys.* **77** 1027 (2005)
116. Kotliar G et al. *Phys. Rev. Lett.* **87** 186401 (2001)
117. LeBlanc J P F et al. *Phys. Rev. X* **5** 041041 (2015)
118. Stanescu T D et al. *Ann. Physics* **321** 1682 (2006)
119. Chen Y-H et al. *Phys. Rev. B* **91** 045122 (2015)
120. Zhang Y Z, Imada M *Phys. Rev. B* **76** 045108 (2007)
121. Kyung B, Tremblay A-M S *Phys. Rev. Lett.* **97** 046402 (2006)
122. Lichtenstein A I, Katsnelson M I *Phys. Rev. B* **62** R9283 (2000)
123. Hettler M H et al. *Phys. Rev. B* **58** R7475 (1998)
124. Maier T A et al. *Phys. Rev. Lett.* **95** 237001 (2005)
125. Gull E, Parcollet O, Millis A J *Phys. Rev. Lett.* **110** 216405 (2013)
126. Aryanpour K, Maier Th A, Jarrell M *Phys. Rev. B* **71** 037101 (2005)
127. Potthoff M, Aichhorn M, Dahnken C *Phys. Rev. Lett.* **91** 206402 (2003)
128. Dahnken C et al. *Phys. Rev. B* **70** 245110 (2004)
129. Aichhorn M et al. *Phys. Rev. B* **74** 235117 (2006)
130. Sénéchal D et al. *Phys. Rev. Lett.* **94** 156404 (2005)
131. Rohringer G et al. *Rev. Mod. Phys.* **90** 025003 (2018)
132. Stratonovich R L *Sov. Phys. Dokl.* **2** 416 (1957); *Dokl. Akad. Nauk SSSR* **115** 1097 (1957)
133. Hubbard J *Phys. Rev. Lett.* **3** 77 (1959)
134. Rubtsov A N, Katsnelson M I, Lichtenstein A I *Phys. Rev. B* **77** 033101 (2008)
135. Rubtsov A N et al. *Phys. Rev. B* **79** 045133 (2009)
136. Rubtsov A N, Katsnelson M I, Lichtenstein A I *Ann. Physics* **327** 1320 (2012)
137. Jaeckel J, Wetterich C *Phys. Rev. D* **68** 025020 (2003)
138. Baier T, Bick E, Wetterich C *Phys. Rev. B* **70** 125111 (2004)
139. Toschi A, Katanin A A, Held K *Phys. Rev. B* **75** 045118 (2007)
140. Maier T A, Jarrell M S, Scalapino D J *Phys. Rev. Lett.* **96** 047005 (2006)
141. Ribic T et al. *Phys. Rev. B* **96** 235127 (2017)
142. Sadovskii M V et al. *Phys. Rev. B* **72** 155105 (2005)
143. Kuchinskii E Z, Nekrasov I A, Sadovskii M V *Phys. Usp.* **55** 325 (2012); *Usp. Fiz. Nauk* **182** 345 (2012)
144. Kitatani M, Tsuji N, Aoki H *Phys. Rev. B* **92** 085104 (2015)
145. Ayral T, Parcollet O *Phys. Rev. B* **92** 115109 (2015)
146. Ayral T, Parcollet O *Phys. Rev. B* **93** 235124 (2016)
147. Vučičević J, Ayral T, Parcollet O *Phys. Rev. B* **96** 104504 (2017)
148. Cao X et al. *Phys. Rev. B* **97** 155145 (2018)
149. Richter M et al. *Phys. Rev. B* **104** 195107 (2021)
150. Sponza L et al. *Phys. Rev. B* **95** 041112 (2017)
151. Vučičević J et al. *Phys. Rev. Lett.* **123** 036601 (2019)
152. Kauch A et al. *Phys. Rev. Lett.* **124** 047401 (2020)
153. Simard O, Takayoshi S, Werner P *Phys. Rev. B* **103** 104415 (2021)
154. Stepanov E A et al. *Phys. Rev. Lett.* **127** 207205 (2021)
155. Ayral T, Vučičević J, Parcollet O *Phys. Rev. Lett.* **119** 166401 (2017)
156. Krien F *Phys. Rev. B* **99** 235106 (2019)
157. Stepanov E A, Harkov V, Lichtenstein A I *Phys. Rev. B* **100** 205115 (2019)
158. Harkov V et al. *Phys. Rev. B* **103** 245123 (2021)
159. Stepanov E A et al. *Phys. Rev. B* **94** 205110 (2016)
160. Krien F, Valli A, Capone M *Phys. Rev. B* **100** 155149 (2019)
161. Stepanov E A et al. *npj Comput. Mater.* **8** 118 (2022)
162. Schäfer T et al. *Phys. Rev. B* **94** 235108 (2016)
163. Chalupa P et al. *Phys. Rev. B* **97** 245136 (2018)
164. Krien F, Valli A *Phys. Rev. B* **100** 245147 (2019)
165. Vandelli M et al. *Phys. Rev. Res.* **5** L022016 (2023)

166. Vandelli M et al. *SciPost Phys.* **13** 036 (2022)
167. Stepanov E A *Phys. Rev. Lett.* **129** 096404 (2022)
168. Bickers N E, in *Theoretical Methods for Strongly Correlated Electrons* (Eds D Sénéchal, A-M Tremblay, C Bourbonnais) (New York: Springer, 2004) Ch. 6, pp. 237–296
169. Tam K-M et al. *Phys. Rev. E* **87** 013311 (2013)
170. Li G et al. *Phys. Rev. B* **93** 165103 (2016)
171. Wentzell N et al. *Phys. Rev. B* **102** 085106 (2020)
172. Eckhardt C J et al. *Phys. Rev. B* **101** 155104 (2020)
173. Krien F et al. *Phys. Rev. B* **102** 195131 (2020)
174. Astretsov G V, Rohringer G, Rubtsov A N *Phys. Rev. B* **101** 075109 (2020)
175. Taranto C et al. *Phys. Rev. Lett.* **112** 196402 (2014)
176. Vilardi D, Taranto C, Metzner W *Phys. Rev. B* **99** 104501 (2019)
177. Metzner W et al. *Rev. Mod. Phys.* **84** 299 (2012)
178. Dupuis N et al. *Phys. Rep.* **910** 1 (2021)
179. Kugler F B, von Delft J *Phys. Rev. Lett.* **120** 057403 (2018)
180. Kugler F B, von Delft J *Phys. Rev. B* **97** 035162 (2018)
181. Hille C et al. *Phys. Rev. Res.* **2** 033068 (2020)
182. Zhu T, Chan G K-L *Phys. Rev. X* **11** 021006 (2021)
183. Rubtsov A N *Phys. Rev. E* **97** 052120 (2018)
184. Rubtsov A N, Stepanov E A, Lichtenstein A I *Phys. Rev. B* **102** 224423 (2020)
185. Lyakhova Ya S, Stepanov E A, Rubtsov A N *Phys. Rev. B* **105** 035118 (2022)
186. Schäfer T et al. *Phys. Rev. X* **11** 011058 (2021)